Climate-driven load shifts and the optimal design of district heating and cooling systems: planning energy supply for a warming century

Jonathan Hachez[a,b,*], Nicolas Ghilain[c], Ali Kök[d], Diederik Coppitters[e]

[a] *Fluid and Thermal Dynamics (FLOW), Vrije Universiteit Brussel, Pleinlaan 2, 1050 Brussels, Belgium*
[b] *Brussels Institute for Thermal-fluid systems and clean Energy (BRITE), Vrije Universiteit Brussel (VUB) and Université Libre de Bruxelles (ULB), Belgium*
[c] *Royal Meteorological Institute of Belgium, Avenue Circulaire 3, B-1180 Brussels, Belgium*
[d] *Energy Economics Group (EEG), Technische Universität Wien, Gußhausstraße 25 – 29 / E370-03, 1040 Vienna, Austria*
[e] *Institute of Mechanics, Materials and Civil Engineering (iMMC), Université catholique de Louvain (UCLouvain), Place du Levant, 2, 1348 Louvain-la-Neuve, Belgium*

Abstract

This paper introduces a multi-stage stochastic optimization framework based on Stochastic Dual Dynamic Programming (SDDP) to plan long-term District Heating and Cooling (DHC) systems under deep climate uncertainty. Integrating Shared Socioeconomic Pathways (SSPs) with uncertain CO2 prices and thermal demands, the framework provides adaptive investment strategies until 2100. Applied to a Belgian case, results project a fundamental shift from heating to cooling, with heat losses declining by up to $-57\% \pm 34\%$ and heat gains increasing by up to $+291\% \pm 25\%$ by 2100 across scenarios. The model consistently converges to robust, electrified configurations dominated by Air-Source Heat Pump (ASHP) and Ground-Source heat pump (GSHP) supported by seasonal Borehole Thermal Energy Storage (BTES), with Natural Gas boiler (NG) relegated to marginal backup roles. While transition mechanisms differ, driven by warming in high-emission pathways and by carbon pricing in mitigation pathways, system costs and emissions converge across scenarios. This work demonstrates that electrified DHC systems with seasonal storage offer a cost-effective, resilient strategy for temperate climates under deep uncertainty, though outcomes are sensitive to regional climate and demand profiles.

Keywords: Robust Design, HVAC, Energy demand projection, Cost optimization, Climate impact on energy, Seasonal thermal energy storage

List of acronyms

ASHP Air-Source Heat Pump

BAIT Building Adjusted Internal Temperature

*Corresponding author
Email address: jonathan.hachez@vub.be (Jonathan Hachez)

BTES Borehole Thermal Energy Storage

CDD Cooling Degree Day

COP Coefficient Of Performance

DHC District Heating and Cooling

GCM Global Circulation Model

GSHP Ground-Source heat pump

HDD Heating Degree Day

JuDGE Julia Decomposition for Generalized Expansion

LP Linear Programming

NG Natural Gas boiler

OPEX Operating Expenses

RCM Regional Climate Model

RCP Representative Concentration Pathway

RHS Right Hand Side

SDDP Stochastic Dual Dynamic Programming

SSP Shared Socio-economic Pathways

SRES Special Report on Emissions Scenarios

VDD Variable Degree Day

Nomenclature

Sets

Symbol	Description
$\mathcal{T}$	set of available technologies
$\mathcal{D}$	set of representative days
$\mathcal{H}$	set of hours composing representative days
$\mathcal{L}_t$	integer set $\{1, ..., L_t + 1\}$ representing the number of stages left for technology t before retirement

Indices

Symbol	Description
t	technology index where $t \in \mathcal{T}$
d	representative day index where $d \in \mathcal{D}$
h	hour index where $h \in \mathcal{H}$
l	remaining lifetime stage index where $l \in \mathcal{L}_t$
ω	scenario index

Decision Variables

Symbol	Unit	Description
$x_{t,l}$	kW	installed capacity of technology t with remaining lifetime l
$x_{t,L+1}$	kW	newly installed capacity of technology t
$y_{t,d,h}$	kW	thermal power output of technology t during day d at hour h
$y^h_{t,d,h}$	kW	heating power output of technology t during day d at hour h
$y^c_{t,d,h}$	kW	cooling power output of technology t during day d at hour h
$T_{d,h}$	°C	indoor temperature of buildings during day d at hour h
$\Delta T^h_{d,h}$	°C	deviation below minimum comfort temperature during day d at hour h
$\Delta T^c_{d,h}$	°C	deviation above maximum comfort temperature during day d at hour h

Parameters

Temperature

Symbol	Unit	Description
$T_{\text{out},d,h}$	°C	outdoor temperature during day d at hour h
$T_{\max,d,h}$	°C	maximum desired indoor temperature during day d at hour h
$T_{\min,d,h}$	°C	minimum desired indoor temperature during day d at hour h
$T^h_{\text{supply},d}$	°C	temperature of supplied heat during day d
$T^c_{\text{supply},d}$	°C	temperature of supplied cold during day d

Building Characteristics

Symbol	Unit	Description
$U_{d,h}$	kW/°C	heat transfer coefficient (wall losses, ventilation) during day d at hour h
$Q_{d,h}$	kW	heat gains/losses independent from temperature (solar, internal) during day d at hour h
I	kW h/°C	thermal inertia of buildings

Technology Characteristics

Symbol	Unit	Description
L_t	stages	standard lifetime of technology t
c	€/kW	cost vector for newly installed capacity
C	kWh/kW	scalar linking BTES capacity and peak power

Operational Costs (Tensor u)

Symbol	Unit	Description
$u_{t,d,h}$	€/kWh	operational cost of running technology t during day d at hour h
$\alpha_d(\omega)$	days/decade	average number of actual days represented by typical day d in scenario ω
$\beta_{t,d,h}$	–	conversion factor (COP,η) for technology t during day d at hour h
$\gamma_t(\omega)$	€/kWh	cost of primary resource for technology t in scenario ω (including CO_2 tax)

Comfort Penalty (Tensor p)

Symbol	Unit	Description
$p_{d,h}$	€/°C	cost of not meeting temperature requirements during day d at hour h
$\gamma_{\text{unmet},d,h}$	€/°C	penalty for thermal discomfort during day d at hour h

Functions

Symbol	Description
$V(\{x_{\cdot,l}\}_{l=1}^{L}, \omega)$	value function representing total cost for a given capacity, state and scenario
$\mathcal{V}_{\text{next}}(\{x_{\cdot,l}\}_{l=2}^{L+1})$	expected value function for next stages

Notation

Superscripts

Symbol	Description
$(\cdot)^h$	heating-related variables
$(\cdot)^c$	cooling-related variables
$(\cdot)^{\text{new}}$	newly installed capacity

Subscripts

Symbol	Description
$(\cdot)_{\text{out}}$	outdoor conditions
$(\cdot)_{\text{min}}$	minimum value
$(\cdot)_{\text{max}}$	maximum value
$(\cdot)_{\text{nom}}$	nominal
$(\cdot)_{\text{supply}}$	supply temperature
$(\cdot)_{\text{unmet}}$	unmet demand or comfort

Operators

Symbol	Description
$\cdot$	dot product or placeholder for all indices
$:$	Frobenius inner product

1. Introduction

Climate change is reshaping energy demand in buildings. Rising temperatures reduce heating needs in colder climates while driving up cooling demand worldwide [1]. These shifts have far-reaching implications for energy systems, infrastructure investments, and climate mitigation goals, since buildings account for around 30% of global final energy use and more than a quarter of energy-related CO_2 emissions [2]. Anticipating how heating and cooling requirements will evolve is therefore a critical challenge for researchers, policymakers, and investors.

Most existing studies address this challenge by projecting how heating and cooling demand respond to alternative climate scenarios [3]. These projections highlight consistent qualitative patterns—declining heating and rising cooling—but differ widely in their quantitative results [4]. Divergence stems from differences in spatial scope, climate scenarios, downscaling methods, and demand modeling approaches [5–7]. The result is a fragmented knowledge base, rich in descriptive insights but difficult to translate into actionable investment strategies.

What is largely missing in this literature is an active perspective: rather than passively describing how demand may shift, one must ask how today's investment decisions can prepare buildings and energy systems for multiple possible futures. Long-lived infrastructure must be robust to deep uncertainty in climate trajectories, socio-economic conditions, and technology adoption. Without frameworks that explicitly link demand projections to adaptive investment planning, stakeholders risk either under-preparing for rising cooling needs or over-investing in solutions that later prove unnecessary.

This article proposes such a framework. We present a method to design investment strategies for district heating and cooling systems that minimize combined operational and investment costs while adapting to uncertain climate-driven demand shifts. To explicitly manage this long-term uncertainty, we employ a capacity expansion model formulated using Julia Decomposition for Generalized Expansion (JuDGE) [8]. This approach leverages SDDP to identify flexible investment strategies that are cost-effective not just for a single forecast, but through different Shared Socio-economic Pathwayss (SSPs). Our climate uncertainty is quantitatively captured through an ensemble of downscaled climate projections, combining multiple Global Circulation Models (GCMs) with a Regional Climate Model (RCM), and is integrated with assumptions on evolving comfort standards to shape future energy demand.

The remainder of the paper is organized as follows. Section 2 reviews existing studies on capacity expansion and climate change impacts on heating and cooling demand, emphasizing methodological choices across spatial scales, climate scenarios, and modeling approaches. Section 3 presents the methodological framework, detailing the stochastic multi-stage programming formulation. Section 4 introduces the case study, describing the location, projected climatic conditions, load characterization, and technology set. Section 5 reports the results, including demand evolution, operational patterns, and optimal investment decisions under different climate scenarios. Section 6 discusses the implications of these results, compares them to existing work, and outlines possible methodological extensions. Finally, Section 7 concludes by summarizing the main findings and highlighting future research directions.

2. Literature review

Our literature review is organized into two main areas. First, we examine recent research on district heating expansion under uncertainty and multi-stage investment frameworks (Section 2.1). Second, we review studies on the evolution of heating and cooling demand under climate change (Section 2.2). Together, these sections highlight a gap in the existing literature, which our work addresses by linking these two research streams to enable long-term planning for long-lifetime assets such as BTES under deep climate uncertainty (Section 2.3).

2.1. District heating network capacity expansion

Capacity expansion for district heating has been studied from multiple perspectives. The most similar work to ours was conducted by Kök et al. [9], who used the package SDDP.jl developed by Dowson and Kapelevich [10]. Leveraging a Markov-chain structure, they performed an SDDP to optimize investment decisions every ten years until 2050, taking into account uncertain operational scenarios. The Markov chain incorporated random evolution in demand and uncertain energy prices, making the algorithm robust to both demand variation and price volatility. More recently, Siddique et al. [11] applied a multistage stochastic optimization framework with risk aversion to the dispatch of large-scale heat-pump-based district heating systems, demonstrating how sequential uncertainty resolution and CVaR-based risk treatment materially affect operational decisions under volatile electricity prices and renewable generation.

Zwickl-Bernhard et al. [12] conducted a two-stage linear programming optimization to meet the energy demand of a district in Washington, D.C. As a first step, they used URBANopt, a framework built on OpenStudio® and EnergyPlus that enabled urban-scale analyses through quasi-dynamic co-simulation. This step provided the area's heating, ventilation, and air-conditioning demand profiles. In the second step, they implemented a two-stage stochastic optimization model, where investment decisions were made in the first stage and energy price volatility was represented in the second stage. Similar methodologies were applied by Shen et al. [13] and Chen et al. [14].

Džiuvė and Lekavičius [15] examined investment options in wastewater heat pump capacity and Power-to-H_2 waste heat solutions under uncertainty in electricity, biofuel, natural gas, and CO_2 prices, as well as heat demand variability. Using the simulation tool EnergyPro, they performed Monte Carlo simulations to identify the best-performing system design and to assess its impact on several technical indicators. Their analysis considered uncertainties projected through 2030.

Grecu et al. [16] investigated the decarbonization of a district heating network in Poland under uncertainty in energy prices (electricity, biomass, and biomethane) and potential waste heat cessation. They used the simulation tool `TESCA`, providing as input the system's heat supply technologies and their capacities, annual residential heat demand, energy carrier prices (electricity, biomass, biomethane, and waste heat), and the temperature levels of ambient and waste heat sources.

Petkov et al. [17] optimized multi-energy systems and envelope retrofits using a deterministic multi-stage optimization framework. They considered 30-year planning horizons with multiple investment periods, allowing the system to adapt as its environment evolved. They performed a multi-objective optimization to minimize CO_2 emissions and costs simultaneously.

Fiorentini et al. [18] optimized a district heating and cooling system incorporating borehole thermal energy storage, showing that optimal BTES sizing and operation depend strongly on boundary conditions such as CO_2 pricing and the availability of cooling-driven waste heat.

2.2. Heating and cooling demand evolution

This section reviews how climate change affects heating and cooling demand in buildings, with a focus on methodological approaches. A study-by-study mapping of scope, scenarios, climate models, horizons, and demand models is provided in Table 1. Time horizons follow the common bins used in the field (2040s, 2050s, 2060s, 2070s, 2080s, 2090s, and 2100s); where relevant, we distinguish between mid-century and late-century results. Although authors make different choices along four interrelated dimensions—spatial scope, scenario framework, climate data and downscaling, and demand models—they converge on the qualitative finding that heating demand decreases and cooling demand increases under warming. The magnitude of change, however, varies widely, and these methodological choices explain much of the divergence.

Global analyses emphasize broad patterns and large-scale uncertainty. Staffell et al. [1] reconstructed demand using MERRA-2 reanalysis data and a Building Adjusted Internal Temperature (BAIT) model, showing that indoor temperature adjustments could deliver substantial energy savings, but also that cooling demand is rising sharply worldwide. Deroubaix et al. [19] combined Heating Degree Day (HDD) and Cooling Degree Day (CDD) with thirty CMIP6 GCMs under two Representative Concentration Pathways (RCPs): RCP 4.5 and 8.5 scenarios; for Paris alone, projected increases in cooling demand ranged from a modest +2% to an extreme +348%, demonstrating the magnitude of climate-model uncertainty. Mastrucci et al. [4] used a global building stock model, coupling SSP–RCP scenarios with a Variable Degree Day (VDD) approach, and showed how assumptions on socio-economic development affect emissions as much as climate trajectories. Earlier, Labriet et al. [20] stressed the feedback loop between global emissions, climate change, and space-conditioning demand, albeit with limited quantitative detail.

At the continental scale, authors rely on ensembles of RCMs to better capture spatial variability. In Europe, Larsen et al. [21] used five RCMs under RCP 2.6, 4.5, and 8.5, combined with HDD/CDD metrics, to project heating reductions of 9–15% and cooling increases of up to 130% by 2050. Spinoni et al. [22], using the same RCM ensemble but extending to 2100, found even sharper changes, emphasizing the role of time horizon in amplifying impacts. Despite differences in magnitude, both studies converge on the finding that heating decreases and cooling increases, though the magnitude depends strongly on the climate scenario.

National-scale analyses typically combine climate projections with more detailed demand models. In Germany, Olonscheck et al. [23] applied Special Report on Emissions Scenarios (SRES) A1B and A2 scenarios with a single RCM to estimate HDD/CDD-based energy demand, highlighting the moderating influence of policy and demographic factors. In Switzerland, Wehrli et al. [24] used the CH2018 climate ensemble with the dynamic IDA-ICE simulation tool, showing that the choice of reference year shifts results significantly. Also in Switzerland, Mutschler et al. [6] applied 68 CH2018 projections under RCP 2.6, 4.5, and 8.5 with HDD/CDD metrics, and concluded that cooling device uptake can outweigh the direct climate signal. For Belgium, Elnagar et al. [3] combined GCM outputs with a single RCM to simulate SSP–RCP pairs, using an analytical building model; they found mid- to late-century heating demand reductions of 13–22% and cooling increases of 61–123% by 2090. In China, Xiong et al. [5] employed DeST building simulations with SSP–RCP combinations, finding surging cooling demand in southern provinces but modest changes in the north. In Portugal, Andrade et al. [25] used seven RCMs under RCP 4.5 and 8.5 to map spatial patterns of HDD/CDD changes, revealing strong intra-country contrasts. Together, these national studies illustrate how choice of scenario framework (SRES vs. RCP vs. SSP–RCP), climate data (ensembles vs. single models), and demand models (degree days vs. building simulations vs. analytical balances) produces different levels of uncertainty.

Regional analyses often use synthetic archetypes to compare climates across areas. Walch et al. [26] evaluated shallow geothermal systems in Vaud and Geneva (Switzerland), linking RCP 2.6, 4.5, and 8.5 scenarios to HDD/CDD demand estimates, and showing that increasing cooling demand stresses seasonal balancing and limits geothermal potential unless complemented by district heating networks. Ziemele et al. [27] quantified how global warming and building renovation jointly reduce heat demand and alter required district heating capacity, illustrating that climate change affects not only energy consumption but also long-term infrastructure adequacy. Inter-regional comparisons highlight climatic diversity: Ahmed et al. [28] simulated a common archetype in Valladolid, Cairo, Brasília, Juneau, and Warsaw using EnergyPlus, revealing minimal change in Alaska but dramatic cooling surges in Cairo. Tomrukcu and Ashrafian [29] used EnergyPlus to compare Izmir and Istanbul under multiple RCPs, with stronger growth in the warmer city. Guarino et al. [30] relied on CESM1(CAM5) GCM projections under RCPs 2.6, 4.5, 6.0, and 8.5, also with EnergyPlus, to contrast Palermo and Copenhagen, finding large absolute increases in southern Europe but steeper relative increases in northern Europe. Similarly, Cellura et al. [7] applied 24 GCMs with TRNSYS across 16 Mediterranean locations, while Rodrigues and Fernandes [31] used SRES A2 scenarios, CCWorldWeatherGen downscaling, and the EPSAP plus EnergyPlus combination to test overheating in southern Europe. Across these studies, the combination of archetype-based building simulation and diverse climate inputs shows how methodological choices interact with geography to shape outcomes.

Local studies provide the most detailed but also the most heterogeneous results, since they depend heavily on building archetype, weather generator, and demand model. In Slovenia, Vidrih and Medved [32] tested multiple heating and cooling techniques with TRNSYS under SRESs A2 and B2, using four GCMs. In India, Thapa et al. [33] simulated a concrete multi-family building in the Himalayas using DesignBuilder/EnergyPlus and CCWorldWeatherGen, showing disproportionate cooling increases due to poor thermal inertia. In Tehran, Aram et al. [34] combined CCWorldWeatherGen with DesignBuilder/EnergyPlus and an NSGA-II optimization to show that passive retrofits can partially offset climate-driven increases. In Sweden, Hosseini et al. [35] used five GCMs under RCPs with a degree-day approach and the Urban Weather Generator, emphasizing the role of extreme events. In Poland, Bazazzadeh et al. [36] simulated ASHRAE 90.1 archetypes with EnergyPlus and CCWorldWeatherGen, while in Milan, P. Tootkaboni et al. [37] used EnergyPlus with 14 GCMs processed through WeatherShift. In Spain, Rey-Hernández et al. [38] simulated buildings with DesignBuilder/EnergyPlus and CCWorldWeatherGen to link demand to renewable integration. In Cameroon, Nematchoua et al. [39] applied HDD/CDD under SRESs A1B, A2, and B1 with 14 GCMs, finding cooling increases dominate. Finally, Summa et al. [40] used TRNSYS with ERA-Interim/UrbClim data to simulate a nearly-zero energy building in Rome, showing that efficiency gains only partly offset rising cooling loads. These local case studies underscore that weather generator choice (CCWorldWeatherGen, WeatherShift, UWG, UrbClim), simulation platform (EnergyPlus, TRNSYS, DesignBuilder, DeST, IDA-ICE), and building archetype assumptions drive as much variation as the climate scenario itself.

Scenario frameworks have evolved alongside these applications. Early national and local studies often used the SRESs, which described divergent socio-economic futures without explicit climate policies [23, 39]. From 2005 onward, these were replaced by RCPs, and most recent continental and global studies combine SSPs with RCPs [4, 5].

The climatic inputs to these scenarios come from different classes of models. GCMs provide large-scale projections and are common in global studies, often in large ensembles; for example, Deroubaix et al. [19] used thirty CMIP6 GCMs to illustrate the scale of uncertainty. By contrast, smaller-scale studies often select a subset of GCMs or downscale them with RCMs, as in European continental work [21, 25] and national assessments based on the CH2018 ensemble [24]. Local studies frequently rely on weather generators to produce hourly weather files for building simulations: CCWorldWeatherGen [31, 33, 36, 38], WeatherShift [37], the Urban Weather Generator (UWG) [35], and ERA-Interim/UrbClim [40]. Results depend strongly on the chosen generator and downscaling chain.

Finally, the way energy demand is modeled varies systematically with scope and data availability. Degree-day methods remain the most widely used for large-scale work because of their simplicity and scalability, but they tend to exaggerate linear trends in response to warming. By contrast, building energy simulation dominates local and case-study analyses—most commonly EnergyPlus and TRNSYS, alongside IDA-ICE and DeST—often coupled with design-generation or optimization tools such as EPSAP [31] and NSGA-II [34]. These models capture non-linearities and extreme events, but their results are highly sensitive to assumptions about building design and operation. Stock models and analytical balances offer a middle ground, particularly suited to national assessments [3].

Table 1: Study-by-study mapping of scope, scenarios, climate models, horizons, and demand models.

Study	**Scope**	**Scenario(s)**	**Climate model(s)**	**Horizon**	**Demand model**
Staffell (2023) [1]	Global	Historical	MERRA-2 reanalysis	1980–2022	BAIT / DD-like
Deroubaix (2021) [19]	Global	RCP4.5, 8.5	30 CMIP6 GCMs	2040s	HDD/CDD
Mastrucci (2021) [4]	Global	SSP1–2.6, 2–4.5, 3–7.0	GCM ensemble	2050s	VDD
Labriet (2015) [20]	Global	-	-	-	-
Larsen (2020) [21]	Continental	RCP2.6, 4.5, 8.5	5 RCMs	2050s	HDD/CDD
Spinoni (2018) [22]	Continental	RCP4.5, 8.5	5 RCMs	2100s	HDD/CDD
Olonscheck (2011) [23]	National	SRESs A1B, A2	1 RCM	2060s	HDD/CDD
Wehrli (2024) [24]	National	RCP2.6, 8.5	CH2018 ensemble	2070s	IDA-ICE
Elnagar (2023) [3]	National	SSP–RCP pairs	GCM + 1 RCM	2100s	Analytical
Xiong (2023) [5]	National	SSP1–2.6, 2–4.5, 3–7.0, 5–8.5	-	2100s	DeST
Andrade (2021) [25]	National	RCP4.5, 8.5	7 RCMs	2070s	HDD/CDD
Mutschler (2021) [6]	National	RCP2.6, 4.5, 8.5	68 proj. (CH2018)	2060s	HDD/CDD
Walch (2022) [26]	Regional	RCP2.6, 4.5, 8.5	-	2050s	GSHP/system
Ahmed (2025) [28]	Inter-regional	-	-	2080s	EnergyPlus
Tomrukcu (2024) [29]	Inter-regional	RCP2.6, 4.5, 8.5	-	2080s	EnergyPlus
Guarino (2022) [30]	Inter-regional	RCP2.6, 4.5, 6.0, 8.5	CESM1(CAM5)	2090s	EnergyPlus
Cellura (2018) [7]	Inter-regional	RCP2.6, 4.5, 6.0, 8.5	24 GCMs	2090s	TRNSYS
Rodrigues (2020) [31]	Inter-regional	SRES A2	-	2050s	EPSAP + EnergyPlus
Vidrih (2008) [32]	Local	SRESs A2, B2	4 GCMs	2050s	TRNSYS
Thapa (2023) [33]	Local	SRES A2	CCWorldWeatherGen	2080s	DesignBuilder / EP
Aram (2022) [34]	Local	SRES A2	CCWorldWeatherGen	2080s	DB/EP; NSGA-II
Hosseini (2022) [35]	Local	RCP2.6, 4.5, 8.5	5 GCMs	2100s	Degree-days
Bazazzadeh (2021) [36]	Local	SRES A2	CCWorldWeatherGen	2080s	EnergyPlus (ASHRAE 90.1)

Continued on next page

Table 1 (continued)

Study	Scope	Scenario(s)	Climate model(s)	Horiz.	Demand model
Tootkaboni (2021) [37]	Local	RCP2.6, 4.5, 8.5	WeatherShift™ (14 GCMs)	2100s	EnergyPlus (TABULA)
Rey-Hernández (2018) [38]	Local	-	CCWorldWeatherGen	2080s	DesignBuilder / EP
Nematchoua (2015) [39]	Local	SRESs A1B, A2, B1	14 GCMs	2070s	HDD/CDD
Summa (2020) [40]	Local	RCP4.5, 8.5	ERA-Interim/UrbClim	2050s	TRNSYS (nZEB)

2.3. Research Gap and Contribution

Across scales, existing climate-related studies consistently find that heating demand decreases and cooling demand increases under climate change. Yet their quantitative results diverge substantially, reflecting differences in spatial scope, scenario frameworks, climate data, downscaling choices, and demand models. In parallel, capacity expansion studies often rely on discrete scenarios that assume demand increases or decreases by a fixed percentage, but these studies typically do not model the explicit, dynamic impact of climate change on demand. The literature thus offers a fragmented picture. It either maps demand trajectories without proposing actionable strategies, or it proposes strategies while ignoring the critical influence of climate change. Crucially, no study addresses how long-lived building and energy-system investments can adapt under such deep uncertainty rooted in climate-driven demand shifts. Instead, authors have passively projected demand changes without exploring how to actively design cost-effective, climate-resilient systems. This article fills that gap by proposing an investment planning framework that accounts for scenario uncertainty and identifies strategies that minimize combined operational and investment costs while remaining adaptive to future needs.

3. Methodology

This section introduces the methodological framework employed to address the investment strategies for building energy systems that minimize combined operational and investment costs while adapting to uncertain climate-driven demand shifts (Section 3.1). Specifically, this section provides the formulation of the stochastic multi-stage programming model, including the implementation of the SDDP algorithm for solving this class of problems and the scenario structures. Section 3.2 applies this framework to our specific problem and introduces the notation, variable definitions, and demand representations.

3.1. Stochastic multi-stage programming

Stochastic multi-stage programming is used to solve Linear Programming (LP) optimization problems constituted of T optimization stages where initial variables must be optimized given v_t possible scenarios and the availability of next-stage variables and parameters. We denote the uncertain parameters for each

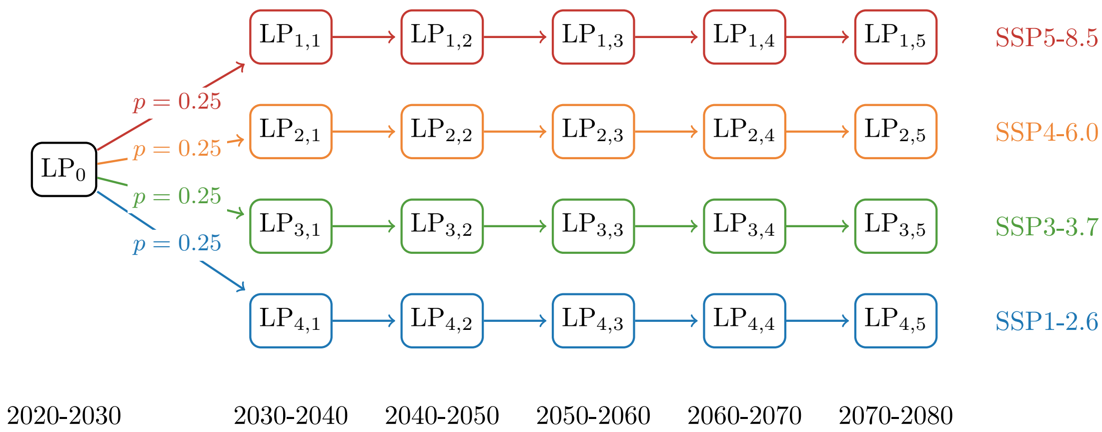

Figure 1: A representation of our problem: each stage represents a decade, and each branch represents a different SSP impacting ambient temperatures and carbon prices evolution. The uncertainty lies between stages 0 and 1, as an SSP is sampled with probability 0.25. Afterwards, each SSP is modelled using the usual deterministic multi-stage modelling.

scenario $\omega_{ti}, t \in 1, ..., T, i \in 1, ..., v_t$. Inter-stage constraints create a relation between stages, making the decision process more complex and increasing the problem's complexity, but the resulting solution is also statistically optimal and takes into account uncertainty [41].

An elegant formulation for a T-stage problem is provided by Philpott and Guan [42]. We adapted it to explicitly separate the investment variables x and the operational variables y in the following:

$$\mathrm{LP}_1 : \quad V_1 = \min_{x_1, y_1} c_1^{\mathrm{T}} x_1 + u_1^{\mathrm{T}} y_1 + \mathcal{V}_2(x_1) \tag{1}$$

$$\text{s.t.} \quad A_1 x_1 + B_1 y_1 = b_1 \tag{2}$$

$$x_1, y_1 \geq 0 \tag{3}$$

$$\mathrm{LP}_{ti} : \quad V_t(x_{t-1}, \omega_{ti}) = \min_{x_t, y_t} c_t^{\mathrm{T}} x_t + u_t^{\mathrm{T}} y_t + \mathcal{V}_{t+1}(x_t) \tag{4}$$

$$\text{s.t.} \quad A_t x_t + B_t y_t = \omega_{ti} - D_{t-1} x_{t-1} \tag{5}$$

$$x_t, y_t \geq 0 \tag{6}$$

where $\mathcal{V}_t(x_{t-1}) = \mathbb{E}[V_t(x_{t-1})] = \sum_{i=1}^{v_{ti}} p_{ti} V_t(x_{t-1}, \omega_{ti})$ for all $t \in 2, ..., T$ and $\mathcal{V}_{T+1} = 0$ where p_{ti} is the transition probability from the current state to state i at stage t.

Several solvers can be used to address this type of problem. In this study, we use the SDDP algorithm through the JuDGE.jl package developed by Baucke et al. [8]. The problem structure is shown in Fig. 1, where each branch represents an SSP—that is, a scenario q_t—and each decade corresponds to an optimization stage.

3.2. Subproblem definition

It is important to highlight the different time scales at which we optimize investment and operation. Typically, our optimization horizon is 80 years. As mentioned, each decade is represented by a node, where a subproblem is solved. Each node uses typical days to represent the operations during a given decade.

Typical days. To capture the intraday dynamics and reduce the problem size, we use representative periods with the TSAM package [43–45]. In our case, we choose to select 16 representative days which will represent the weather throughout the century, SSP and GCM[1]: instead of optimizing 365 days $\times$ 80 years $\times$ 6 GCM $\times$ 4 SSP $= 7e5$ days, we optimize 16 representative days of operations whose weight depends on the expected number of occurences (inter-model frequency) they have for each stage (decade) and state (SSP). Per decade, this represents a complexity reduction by a factor of 1368 (from 10 years and 6 models to 16 days). Additional information is available in Appendix B.

3.2.1. Sets and variables

To simplify our notations, we will consider here only the subproblem-specific variables x and y and drop the indices related to stages and scenarios. Similarly, we change the meaning of ω as a stage-state index for an uncertain parameter. In our work, it will serve to highlight the parameters that are scenario-dependent. To do so, we consider four different sets: $\mathcal{T}$ refers to the set of available technologies, $\mathcal{D}$ refers to a set of representative days, and $\mathcal{H}$ is the set of hours composing these representative days. In addition, we define an integer set for each technology $\mathcal{L}_t = \{1, ..., L_t + 1\} \forall t \in \mathcal{T}$ representing the number of stages left for every technology before it retires, where L_t is the standard lifetime of a technologies $t \in \mathcal{T}$ (expressed in number of stages) and the integer $L_t + 1$ indicates that the capacity is being installed, yet not operational.

For each subproblem, $x_{t,l}$ denotes the installed capacity of technology t with remaining lifetime $l \in \mathcal{L}_t$.[2] During typical day d at time h, $y_{t,d,h}$ represents the thermal power output of technology t and $T_{d,h}$ represent the indoor temperature of the buildings.[3]

[1]There are two reasons to keep the same representative days across scenarios and decades: (1) it ensures fair comparison can be done when comparing operation. (2) it allows the use of more advanced techniques (adaptive oracles and bounding techniques)

[2]In particular, JuDGE.jl allows putting a delay and a lifetime (expressed in stages) to install new capacities and how long they will be usable. Again, to simplify notation, we assume that the investment variables x of Eqs. (1), (2), (4) and (5) indicate how much capacity is currently available, depending on the required stages for installation and their estimated lifetime, and we use x_i^{new} to denote the newly installed capacity.

[3]Note that there is no variable y for the BTES technology, as the thermal output of the latter depends on the capacity of the GSHP.

3.2.2. Parameters

In addition to the investment cost vector c, the model utilises the following parameters, defined for each typical day $d \in \mathcal{D}$ and typical hour $h \in \mathcal{H}$.

Temperatures (°C)

- $T_{\text{out},d,h}$: outdoor temperature.
- $T_{\text{max},d,h}$: maximum desired indoor temperature.
- $T_{\text{min},d,h}$: minimum desired indoor temperature.
- $T^{\text{h}}_{\text{supply},d}$: heat supply temperature.
- $T^{\text{c}}_{\text{supply},d}$: cold supply temperature.

Heat Gains and Losses

- $U_{d,h}$: temperature-dependent gain/loss coefficient (kW/°C), accounting for envelope and ventilation losses.
- $Q_{d,h}$: temperature-independent gain/loss (kW), from solar and internal sources.

Cost Tensors Two core cost tensors, u (operational) and p (unmet comfort), are defined as follows.

Tensor u – Operational Costs. The element $u_{t,d,h}$ represents the cost of operating technology t during typical day d at hour h. It is computed as:

$$u_{t,d,h}(\omega) = \frac{\alpha_d(\omega) \cdot \gamma_t(\omega)}{\beta_{t,d,h}} \quad \forall (t,d,h) \in \mathcal{T} \times \mathcal{D} \times \mathcal{H} \tag{7}$$

where

- $\alpha_d(\omega)$ is the average number of actual days represented by typical day d in scenario ω,
- $\beta_{t,d,h}$ is the conversion factor (e.g., Coefficient Of Performance (COP)) from primary resource to useful heat or cold,
- $\gamma_t(\omega)$ is the scenario-dependent cost of the primary resource (including CO_2 taxes).

Tensor p – Unmet Comfort Penalties. Similarly, the element $p_{d,h}$ denotes the cost of deviating from the desired temperature bounds during typical day d at hour h[4]. It is defined as the product:

$$p_{d,h}(\omega) = \alpha_d(\omega) \cdot \gamma_{\text{unmet},d,h} \tag{8}$$

where $\gamma_{\text{unmet},d,h}$ is the penalty per degree of unmet comfort (e/°C). In this study, a fixed penalty of $1\,\text{M€}/°\text{C} \cdot \text{h}$ is applied, effectively enforcing strict comfort requirements.

[4]We refer to Appendix C for more details on the values of β and γ.

3.2.3. Objective function

The objective function of the subproblem, therefore, becomes[5] [6]:

$$V(\{x_{\cdot,l}\}_{l=1}^{L}, \omega) = \min_{x_{\cdot,L+1},y} \quad \underbrace{c \cdot x_{\cdot,L+1}}_{\text{newly installed capacity}} + \underbrace{u(\omega) : y}_{\text{operational cost}} + \underbrace{p : \Delta T}_{\text{thermal discomfort}} + \underbrace{\mathcal{V}_{\text{next}}(\{x_{\cdot,l}\}_{l=2}^{L+1})}_{\text{next stages expected value}} \tag{9}$$

3.2.4. Constraints

Indoor temperature requirements. The main constraint of our model relies on the definition of the comfort interval: we assume an indoor comfort interval ($[T_{\min,d,h}, T_{\max,d,h}]$) for temperature in our model. We assume this interval is $[15\,°\text{C}, 25\,°\text{C}]$ if $h \in [8, 20]$ and $[9\,°\text{C}, 30\,°\text{C}]$ otherwise (assuming the buildings are unoccupied). Accordingly, we define the variables $\Delta T^{\text{h}}_{d,h}$ and $\Delta T^{\text{c}}_{d,h}$ as being the deviations from the interval, which lead to penalties.[7]

$$T_{d,h} + \Delta T^{\text{h}}_{d,h} \geq T_{\min,d,h} \qquad \forall (d,h) \in \mathcal{D} \times \mathcal{H} \tag{10}$$

$$T_{d,h} - \Delta T^{\text{c}}_{d,h} \leq T_{\max,d,h} \qquad \forall (d,h) \in \mathcal{D} \times \mathcal{H} \tag{11}$$

Thermal balance. The thermal balance constraints compute the evolution of the indoor temperature depending on the system operations (heating or cooling) and exogenous factors (heat gains/losses). This formulation makes the building behave like a thermal storage whose temperature can be adapted to reduce costs while keeping in the comfort zone.

$$\underbrace{I \cdot (T_{d,h+1} - T_{d,h})}_{\text{buildings temperature change}} = \underbrace{\sum_{t \in \mathcal{T}} y^{h}_{t,d,h}}_{\text{heating power}} - \underbrace{\sum_{t \in \mathcal{T}} y^{c}_{t,d,h}}_{\text{cooling power}} + \underbrace{U_{d,h} \cdot (T_{\text{out},d,h} - T_{d,h}) + Q_{d,h}}_{\text{gains/losses}} \quad \forall (d,h) \in \mathcal{D} \times \mathcal{H} \tag{12}$$

Heating and cooling supply temperatures are computed daily:

$$T^{\text{h}}_{\text{supply},d} = \max_{h}(T_{\min,d,h} + \max(T_{\min,d,h} - T_{\text{out},d,h}, 0)) + 5 \qquad \forall d \in \mathcal{D} \tag{13}$$

$$T^{\text{c}}_{\text{supply},d} = \min_{h}(T_{\max,d,h} - \max(T_{\text{out},d,h} - T_{\max,d,h}, 0)) - 5 \qquad \forall d \in \mathcal{D} \tag{14}$$

[5]The reader will notice how the vector x is shifted at each stage, leading to a technology pipeline where technology ages through stages.

[6]The operator $\cdot : \cdot$ is a tensor contraction or (Frobenius) inner product. In other words, $u : y$ is equivalent to

$$\sum_{(t,d,h) \in \mathcal{T} \times \mathcal{D} \times \mathcal{H}} u_{t,d,h} \cdot y_{t,d,h}$$

[7]Since these quantities are minimized, they will always be zero except when $T_{d,h}$ deviates from $[T_{\min,d,h}, T_{\max,d,h}]$.

Installed capacity x and thermal output y. The constraints on the maximal capacity are noted leveraging the thermal conversion factor $\beta_{t,d,h}$ and the nominal conversion factor β_{nom} (nominal COP, efficiency) of a technology t on day and time d, h. Leveraging the conversion factor allows considering the limitation in compressor power in heat pumps when temperature gap widens between the heat sink and the sources.

$$\underbrace{\frac{y_{t,d,h}}{\beta_{t,d,h}}}_{\text{operational input}} \leq \underbrace{\frac{\sum_{l\in\mathcal{L}_t\setminus\{L_t+1\}} x_{t,l}}{\beta_{\text{nom}}}}_{\text{nominal input}} \qquad \forall(t,d,h) \in \mathcal{T}\times\mathcal{D}\times\mathcal{H} \tag{15}$$

Geothermal balancing. In practice, a BTES system requires balancing over each subproblem. This means that as much heat has to be sent in as extracted, taking into account the active system contribution to the thermal energy balance. We denote $y^{\text{h}}_{\text{geo},d,h}$ and $y^{\text{c}}_{\text{geo},d,h}$ as the heat and cold generated due to the borehole storage. With $\beta_{\text{geo},d,h}$ denoting the active system's COP, the balancing constraint becomes:

$$\underbrace{\sum_{(d,h)\in\mathcal{D}\times\mathcal{H}} \alpha_d(\omega) y^{\text{h}}_{\text{geo},d,h} \frac{\beta^{\text{h}}_{\text{geo},d,h}-1}{\beta^{\text{h}}_{\text{geo},d,h}}}_{\text{heat extracted from the ground}} = \underbrace{\sum_{(d,h)\in\mathcal{D}\times\mathcal{H}} \alpha_d(\omega) y^{\text{c}}_{\text{geo},d,h} \frac{\beta^{\text{c}}_{\text{geo},d,h}+1}{\beta^{\text{c}}_{\text{geo},d,h}}}_{\text{heat injected in the ground}} \tag{16}$$

Geothermal energy limit. In order to limit the soil variations in temperature, we limit the amount of heat that can be injected into the ground by linking the installed capacity to the maximal amount of energy stored in the ground with a parameter C (see Appendix D.2 for more details).

$$\underbrace{\sum_{(d,h)\in\mathcal{D}\times\mathcal{H}} \alpha_d(\omega) y^{\text{h}}_{\text{geo},d,h} \frac{\beta^{\text{h}}_{\text{geo},d,h}-1}{\beta^{\text{h}}_{\text{geo},d,h}}}_{\text{heat extracted from the ground}} \leq \underbrace{C \cdot \sum_{l\in\mathcal{L}_t\setminus\{L_t+1\}} x_{\text{BTES},l}}_{\text{thermal capacity}} \tag{17}$$

3.2.5. Full Subproblem formulation

Leveraging Eqs. (9) to (12) and (15) to (17) we can write the subproblem as:

$$\min_{x_{\cdot,L+1},y} c \cdot x_{\cdot,L+1} + u(\omega) : y + p : \Delta T + \mathcal{V}_{\text{next}}(\{x_{\cdot,l}\}_{l=2}^{L+1})$$

$$I \cdot (T_{d,h+1} - T_{d,h}) = \sum_{t\in\mathcal{T}} y^h_{t,d,h} - \sum_{t\in\mathcal{T}} y^c_{t,d,h} + U_{d,h} \cdot (T_{\text{out},d,h} - T_{d,h}) + Q_{d,h} \qquad \forall(d,h) \in \mathcal{D}\times\mathcal{H}$$

$$T_{d,h} + \Delta T^{\text{h}}_{d,h} \geq T_{\min,d,h} \qquad \forall(d,h) \in \mathcal{D}\times\mathcal{H}$$

$$T_{d,h} - \Delta T^{\text{c}}_{d,h} \leq T_{\max,d,h} \qquad \forall(d,h) \in \mathcal{D}\times\mathcal{H}$$

$$\frac{y_{t,d,h}}{\beta_{t,d,h}} \leq \frac{\sum_{l\in\mathcal{L}_t\setminus\{L_t+1\}} x_{t,l}}{\beta_{\text{nom}}} \qquad \forall(t,d,h) \in \mathcal{T}\times\mathcal{D}\times\mathcal{H}$$

$$\sum_{(d,h)\in\mathcal{D}\times\mathcal{H}} \alpha_d(\omega) y^{\text{h}}_{\text{geo},d,h} \frac{\beta^{\text{h}}_{\text{geo},d,h}-1}{\beta^{\text{h}}_{\text{geo},d,h}} = \sum_{(d,h)\in\mathcal{D}\times\mathcal{H}} \alpha_d(\omega) y^{\text{c}}_{\text{geo},d,h} \frac{\beta^{\text{c}}_{\text{geo},d,h}+1}{\beta^{\text{c}}_{\text{geo},d,h}}$$

$$\sum_{(d,h)\in\mathcal{D}\times\mathcal{H}} \alpha_d(\omega) y^{\text{h}}_{\text{geo},d,h} \frac{\beta^{\text{h}}_{\text{geo},d,h}-1}{\beta^{\text{h}}_{\text{geo},d,h}} \leq C \cdot \sum_{l\in\mathcal{L}_t\setminus\{L_t+1\}} x_{\text{BTES},l}$$

It is interesting to note at this stage that the only uncertainty in each subproblem translates into an uncertain cost parameter (and an uncertain coefficient for the borehole balancing and limits). Indeed, due to the typical demand days, we could remove the uncertain demand from the Right Hand Side (RHS) term and put it as an uncertain number of times a typical demand would need to be satisfied. Similarly, the uncertain CO_2 tax impacts the objective function, but not the constraints themselves.

4. Case study

This section introduces the case study used to apply and evaluate the proposed methodology. We first describe the location and climate projections that define the boundary conditions of the problem (Section 4.1). Then, we present the building load profiles (Section 4.2) and the set of technologies considered in the analysis (Section 4.3), along with their investment and operational characteristics.

4.1. Location

The case study focuses on Brussels, Belgium (4.3755° E, 50.8620° N) and is located on a campus under renovation of the Vrije Universiteit Brussel. As detailed in Appendix A, the buildings are currently undergoing a change in use, significant retrofitting, and the installation of a brand new DHC system. These concurrent transformations make data-driven methods challenging for this site. The campus network is shown in Fig. 2a, connecting multiple buildings. (see details in Appendix A) Currently, an ASHP feeds the district heating and cooling network, which operates at low temperatures (<60°C), leading to negligible thermal losses. The same distribution infrastructure is used year-round, alternating between supplying heating in the winter and cooling in the summer to the building's active induction beams.

To assess projected temperature changes, we used the RCM *MARv3.14*, which is driven by six GCMs: CMCC-CM2-SR5, EC-Earth3-Veg, IPSL-CM6A-LR, MIROC6, MPI-ESM1-2-HR, and NorESM2-MM. Weather projections were obtained for four shared socioeconomic pathways (SSPs)—SSP1-2.6, SSP2-4.5, SSP3-7.0, and SSP5-8.5—covering the period 2015–2100. The resulting temperature projections for Brussels are shown in Fig. 2b (yearly averaged) and in Fig. 3 (daily average).

4.2. Thermal gains, losses and inertia

The building is subject to various heat gains and losses and has a defined inertia that impacts its thermodynamics. We consider in this article the thermal exchanges with the exterior through envelope and ventilation, the thermal gains due to solar radiation and internal loads and the thermal inertia of the building. The details on the building topology and afferent assumptions are provided in Appendix A. The quantified losses are available in Appendix E.

(a) Representation of the campus' district heating and cooling network. The temperature of the network is adapted such that heating and cooling are delivered alternatively, depending on the season. Supplied buildings are in orange. BTES drilling area is represented in green. Inspired by Anyoji Beltrando Architectes Urbanistes et al. [46]

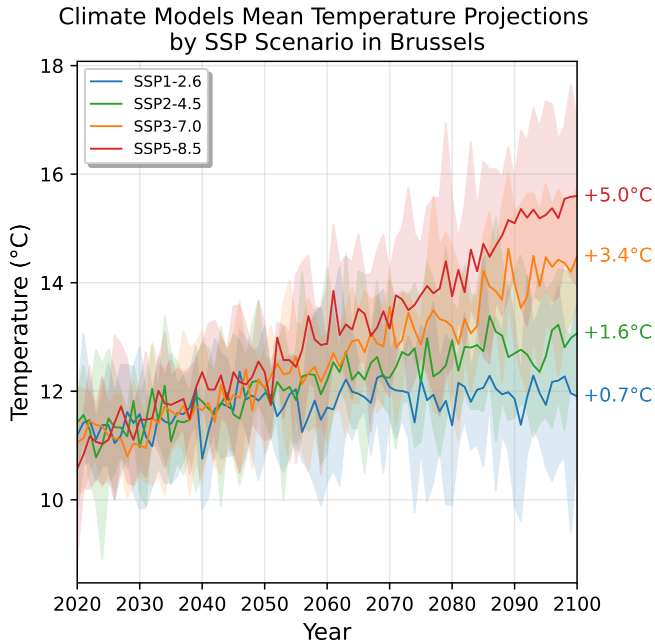

(b) projected yearly averaged outdoor temperature. The solid line represents the inter-model mean, and the shaded area, the dispersion of values across models. The annotation on the right represents the difference between the mean projected temperature in 2020 and 2100.

Figure 2: Characteristics of the case studying Brussels (4.3755°E, 50.8620°N): system lay-out and weather conditions' projection.

4.3. Technologies

The investment costs are derived from Prognos AG et al. [47] and their costs are extrapolated for the end of the century (see method in Appendix D.1). The final costs are visible on Fig. 4.

All investments are subject to a one-decade delay between the investment decision and the availability of the corresponding capacity. All technologies have a technical lifetime of two decades, except for borehole systems, which have a lifetime of five decades.[8] The operational cost u required for the thermal power (heating and cooling) is the product of factors α, β, γ (as detailed in Section 3.1). More details on the computation of β and γ and the influence of the carbon tax are provided in Appendix C.

The optimization starts in 2020 with all heating and cooling demand covered by ASHP capacity. This initial system operates until 2030, when it reaches end-of-life and requires replacement. The model then determines optimal subsequent investments and operations from this starting condition.

[8]To prevent a bias against technologies with long lifespans that are installed near the end of the simulation period, we use a "sandwich cost" method. This ensures that the model fairly values their full lifetime benefits, even beyond the model's time horizon.

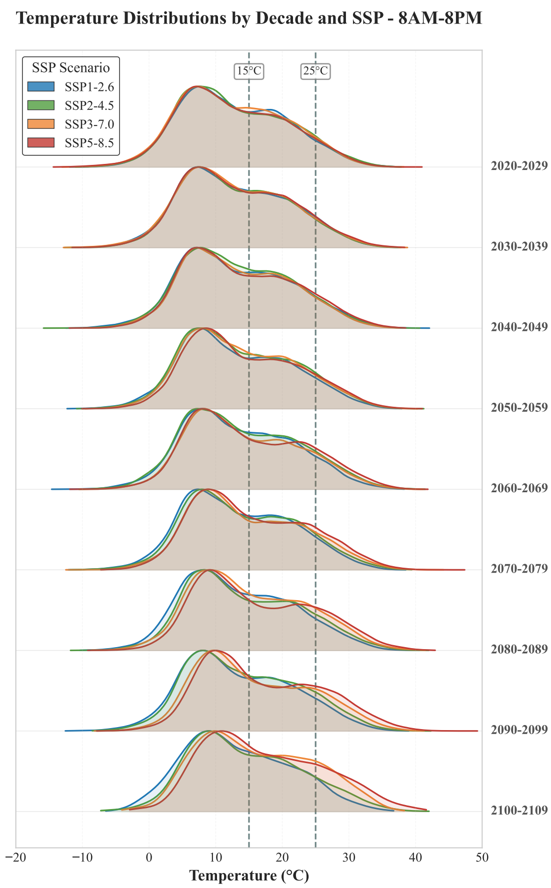

(a) Day distribution

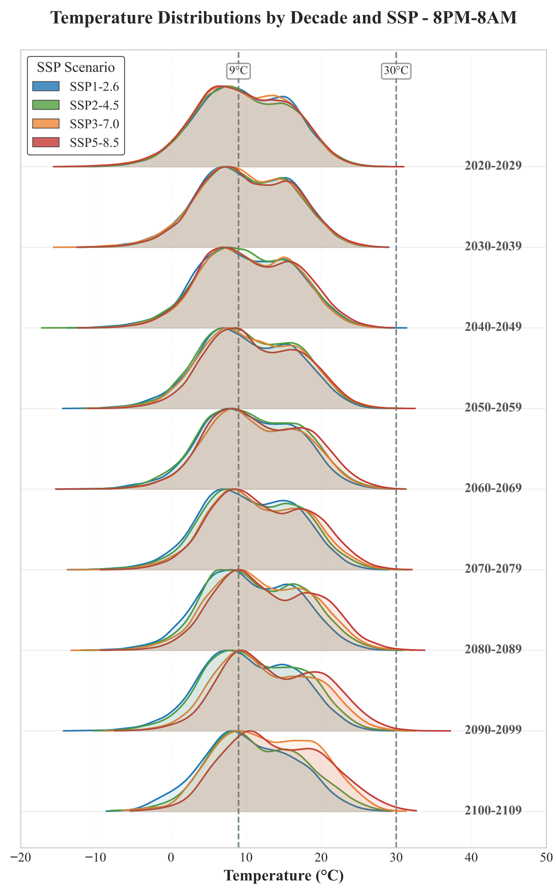

(b) Night distribution

Figure 3: Distribution of the daily-averaged temperature forecast for different decades and ssp. The vertical line indicates the bounds of the indoor comfort interval.

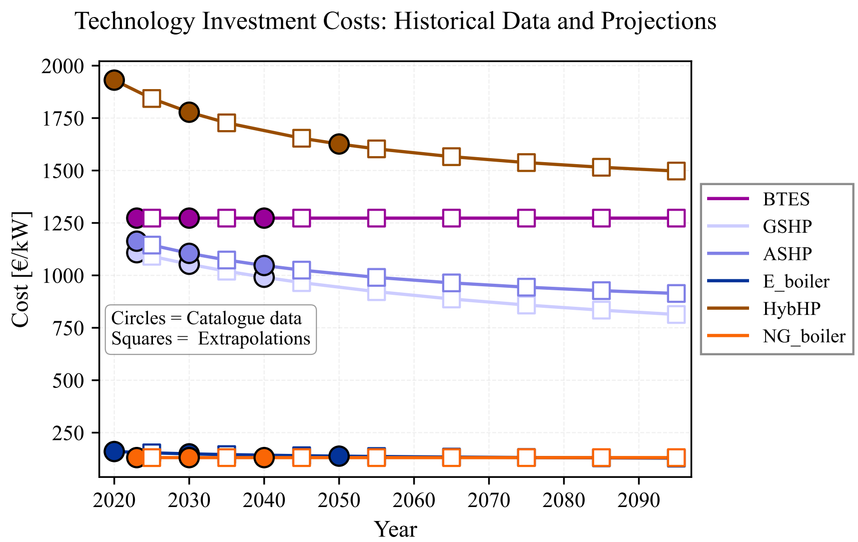

Figure 4: Technology investment cost trajectories. Circles denote historical data points (2010–2023); squares indicate decadal extrapolations (2025–2095). Solid lines show fitted hyperbolic decay curves, capturing technology learning rates and asymptotic cost floors.

5. Results

This section presents the results obtained from applying the proposed methodology to the case study. We first analyze the evolution of heating and cooling demand under different climate scenarios (Section 5.1). We then introduce our objective function decomposition into CAPEX, OPEX and CO_2 costs in Section 5.2. Then, we discuss the resulting optimal technology mix and its evolution across decades and SSPs (Section 5.3), followed by the optimal operational patterns and cost structures that emerge from the model (Section 5.4).

5.1. Evolution of heat gains and losses

Figure 5 illustrates how daily aggregated heat gains and losses needs evolve throughout decades and under the four SSP scenarios. In the 2020s, the heat losses are around 1890 MWh (mainly in winter), while the heat gains remains small, around 715 MWh (mainly in summer). These values reflect the current climate of Brussels, where winters still dominate the thermal balance and cooling demand is almost negligible, despite internal and solar gains. As temperatures rise, however, the relationship between heat gains and losses gradually reverses. Heat losses decreases steadily in all scenarios, falling to about 1730 MWh ($-4\% \pm 23\%$) under SSP1–2.6, 1478 MWh ($-20\% \pm 25\%$) under SSP2–4.5, 1003 MWh ($-49\% \pm 27\%$) under SSP3–7.0, and 845 MWh ($-57\% \pm 34\%$) under SSP5–8.5 by the 2090s. Even under moderate warming (SSP2), heating needs drop by roughly one-fifth, and under severe warming they are effectively halved (SSP3 and SSP5).

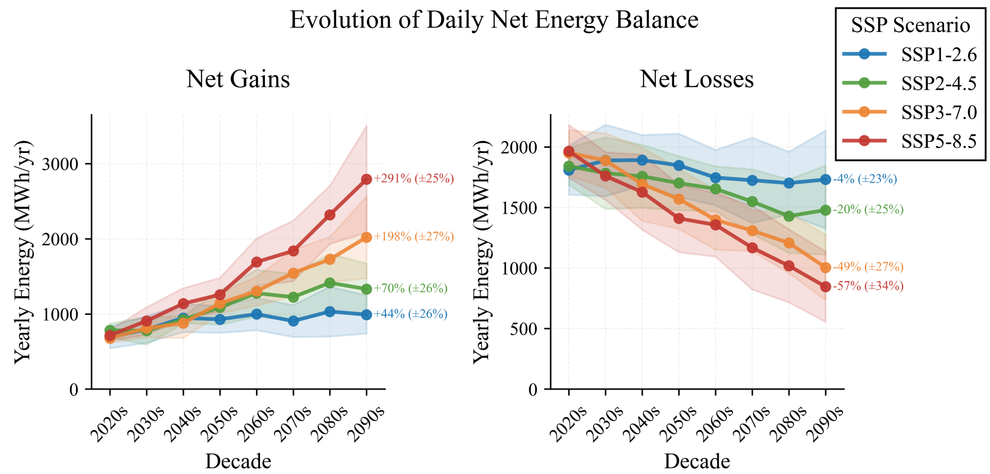

Figure 5: Evolution of net energy balances across SSP scenarios. For each decade, daily energy balances are computed (gains minus losses), then separated into positive (net gains, left) and negative balances (net losses, right). The plots show how the yearly aggregated values evolve under different climate pathways.

This steady decline reflects both shorter heating seasons and smaller temperature differences between indoor and outdoor conditions during winter months.

Cooling demand follows the opposite trend. Starting from about 715 MWh in the 2020s, it rises to approximately 991 MWh (+44% ± 26%) for SSP1–2.6, 1330 MWh (+70% ± 26%) for SSP2–4.5, 2020 MWh (+198% ± 27%) for SSP3–7.0, and 2791 MWh (+291% ± 25%) for SSP5–8.5 by the end of the century. The increase is nearly exponential beyond mid-century, when warming accelerates, and extreme summer conditions become more frequent. In lower-emission scenarios, the rise in cooling demand remains moderate because temperature peaks stay within current comfort thresholds for most of the year.

5.2. *Objective function*

The objective function represents the system's expected total cost, calculated as the average across all scenarios shown in Fig. 6. Results indicate that the objective function decreases as climate change intensifies, with periodic asset renewal every twenty years. The CO2 tax has a minimal impact on overall costs, while investment accounts for more than 50% across scenarios — a proportion that remains relatively stable. The rest of the total costs are attributed to primary resource expenditures (electricity and gas).

5.3. *Optimal design*

Figure 7 illustrates the evolution of installed capacities across the four SSPs. The system exhibits consistent investment patterns across scenarios, reflecting that the use of identical typical days for each decade and SSP enables coverage of similar extreme conditions, despite changes in their frequency.

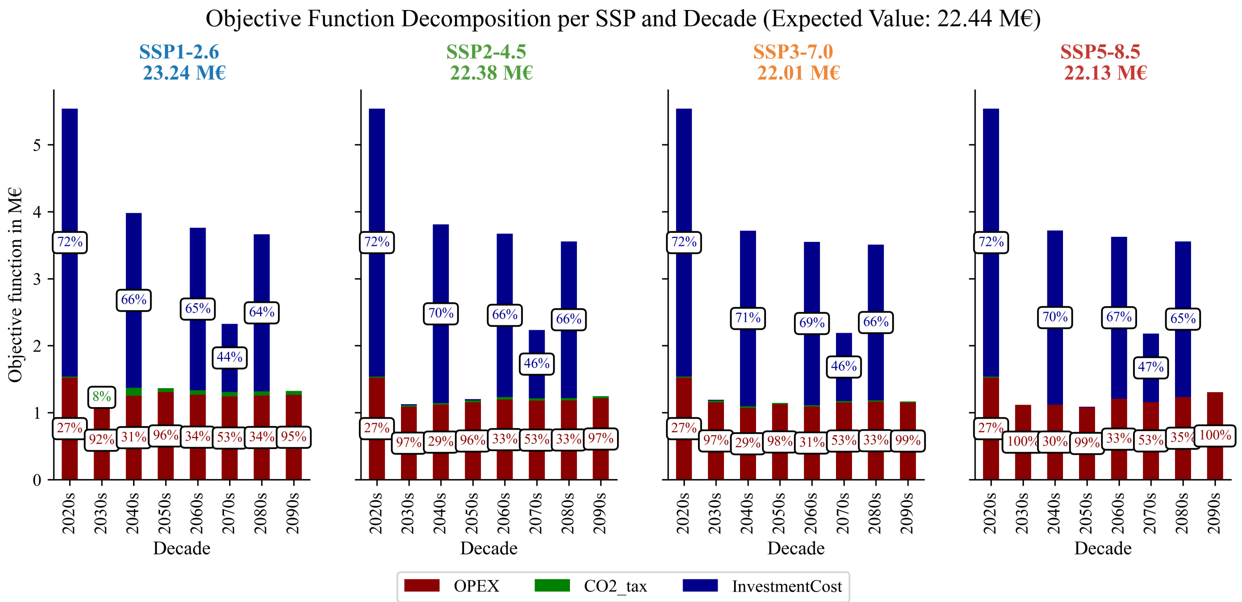

Figure 6: Decomposition of the total discounted objective function across SSPs, decades, and cost categories, explicitly including discounted operational expenditures (OPEX) alongside investment costs and CO_2 taxes.

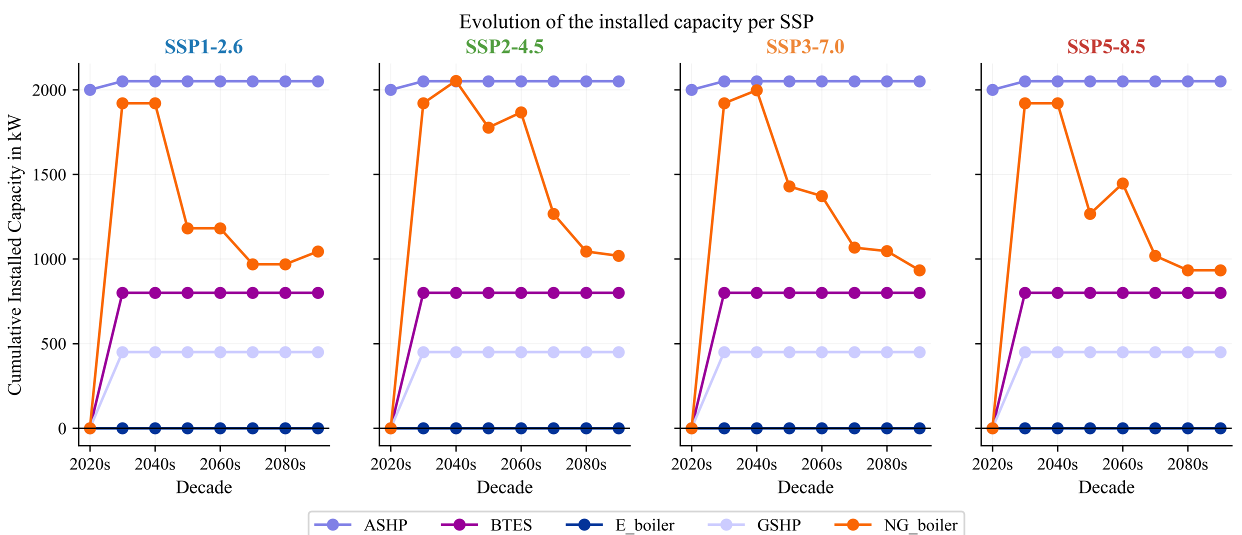

Figure 7: Installed capacities as a function of time and SSP. Power values are reported in equivalent thermal power at the nominal operating point ($T_{\text{out}} = 7\,^{\circ}\text{C}$, $T^{\text{h}}_{\text{supply}} = 35\,^{\circ}\text{C}$).

GSHP reaches saturation rapidly as the most efficient technology, while ASHP maintains a fixed size dictated by cooling peaks. NG capacity initially expands in the second decade as a cost-effective heating solution under harsh winter conditions, then gradually declines in all scenarios.

BTESs saturate at a level constrained by the available drilling power capacity under the given assumptions (see Appendix D.2). In practice, this implies that further expansion would require either a larger drilling area or increased borehole depth.

The only design variable that shows substantial variation is NG capacity, which declines progressively due to: (1) rising CO_2 taxes and electricity decarbonisation in low-emission scenarios, and (2) milder winters in high-emission scenarios.

By the end of the century, the combined nominal capacity exceeds 3750 MW.[9]

5.4. Optimal operations

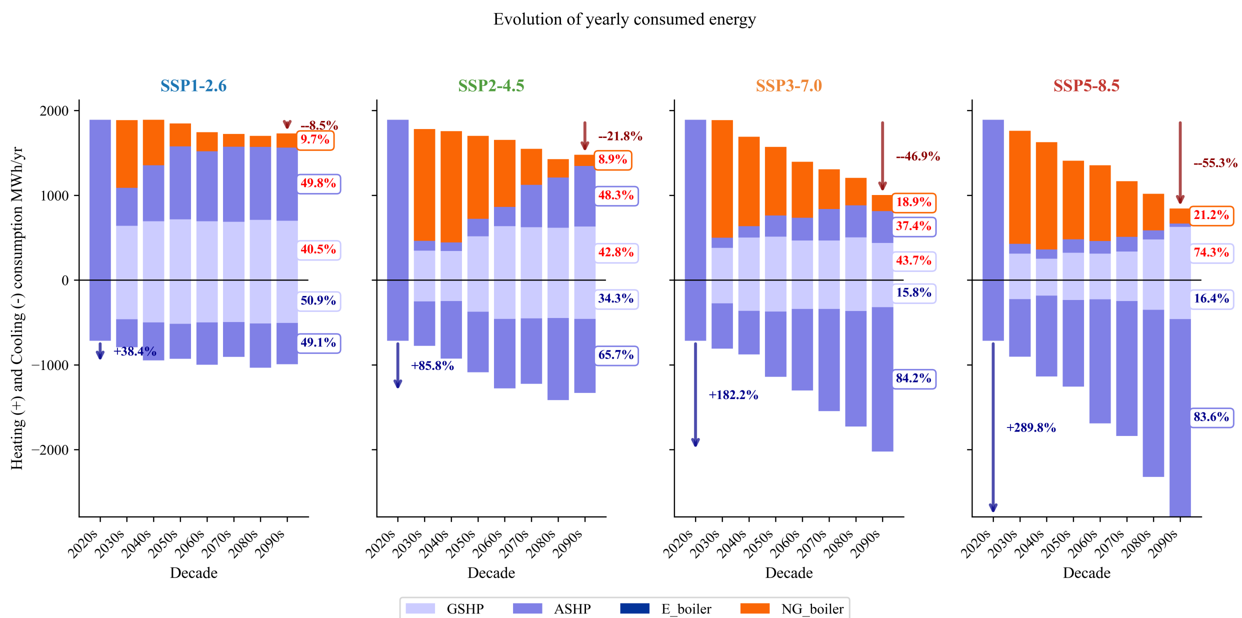

Figure 8: Annual heating and cooling supplied by technology across SSPs and decades. Heating demand decreases as warming intensifies, while cooling grows from marginal to dominant in severe scenarios. Results for 2020 correspond to the initialised system, where heating and cooling are fully met by ASHP.

Energy. Figure 8 presents the annual energy supplied by each technology over time and across SSPs. Although design choices are similar across scenarios, operation is strongly influenced by changing climatic condi-

[9]Nominal conditions correspond to $T_{\text{out}} = 7\,°\text{C}$ and $T^{\text{h}}_{\text{supply}} = 35\,°\text{C}$. The thermal capacities must be interpreted with caution, as the limiting factor for heat-pump assets is typically the primary input (electrical power) rather than the thermal output, and extreme operating conditions reduce effective capacity.

tions and operating costs. Heating and cooling demands remain stable in the mitigation scenario (SSP1-2.6), but gradually shift toward greater cooling as climate change intensifies, resulting in a cooling-dominated system in severe warming pathways (SSP5-8.5).

Heating is primarily supplied by GSHP or NG in early decades, with ASHP playing a minor role. This is due to similar operating conditions, making gas much more competitive than electricity (carbon-intensive electricity mix, low carbon prices) and the relative similarity in climate at that stage. By the end of the century, the pattern diverges:

- In mitigation scenarios, rising CO2 taxes progressively reduce NG use; heating is first met by GSHP until saturation, then by ASHP, with NG reserved only for peaking during extreme cold periods.
- In high-emission scenarios, NG acts as a secondary technology, covering most heating needs not met by saturated GSHP capacity.

Cooling is initially shared equally between ASHP and GSHP. Across all scenarios, GSHP is used until saturation, after which ASHP serves as the flexible secondary technology—its installed capacity remains fixed, but its operating frequency increases with demand.

Interpreting these results is challenging due to the asymmetric shift in demands: heating decreases by 55 % in high-emission scenarios, while cooling increases by over 289 %. This transformation of the heating–cooling balance fundamentally alters the optimal technology mix, favouring flexible cooling solutions and seasonal heat-storage systems as warming intensifies.

Operational Expenditures. Figure 9 shows the evolution of annualized Operating Expenses (OPEX) across decades and SSPs. Total OPEX remains relatively stable across scenarios, but its composition shifts fundamentally with changes in the energy mix and in heating and cooling demand.

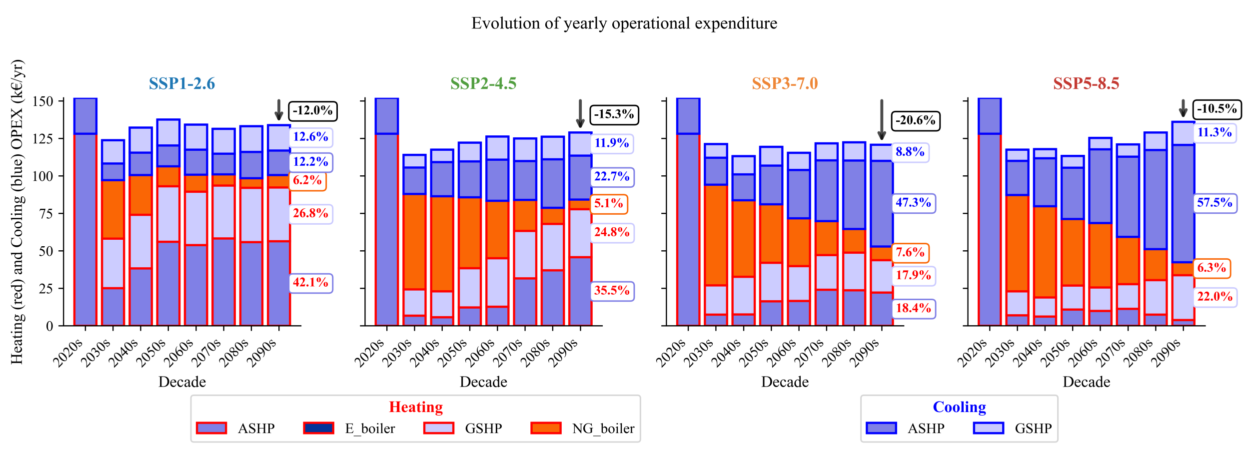

Figure 9: Evolution of annual operational expenditures by source and end-use (heating/cooling) across SSPs.

In the early decades (2030s), heating dominates demand, and cooling is marginal. By the end of the century, outcomes diverge: in mitigation scenarios (SSP1-2.6), heating still drives most costs (75.1 %), whereas in severe warming pathways (SSP5-8.5) cooling becomes the dominant cost component (68.8 %).

NG use declines rapidly around 2050 in SSP1-2.6, due to a carbon-neutral electricity grid and high carbon prices. However, it remains substantial in higher-emission scenarios, where it competes with GSHP for the remaining heating load. In mitigation scenarios, electricity-based heat production accounts for more than 93 % of OPEX, highlighting how high electricity prices can limit full electrification in other pathways.[10] In higher-emission scenarios, heating continues to rely on NG until progressively milder winters reduce its necessity.

CO_2 Emissions. Figure 10 shows the evolution of the carbon emissions of the system over time. Since the electricity grid reaches carbon neutrality by 2050, all operational CO_2 emissions stem from marginal natural-gas use. Results show that CO_2 emissions decline over time, driven either by rising carbon prices or by shrinking heating demand. Nevertheless, the system does not fully decarbonize due to the retained gas boiler for peak loads: despite the technical feasibility of electric boilers, the large energy-cost differential prevents their adoption under optimality conditions, even under high CO_2 prices.

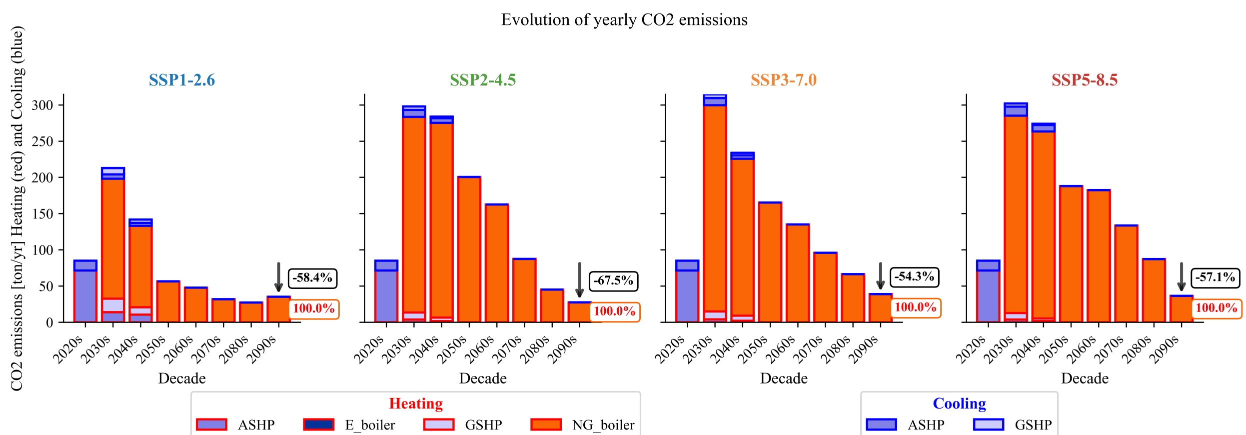

Figure 10: Evolution of the carbon emissions across SSP and decades, decomposed based on their origin.

6. Discussion

The discussion is organized into three parts. Section 6.1 explains how the model behaves and why certain patterns—such as the shift toward electrification and greater use of thermal storage—emerge across climate

[10]Although OPEX appears stable across scenarios, the investment cost of a NG boiler is roughly one-tenth that of an ASHP and one-twentieth that of a GSHP.

scenarios. Section 6.2 compares these findings with results from previous studies, showing where they align and where they differ. Section 6.3 then considers what these results mean for future district heating and cooling planning, notes the main limitations of the current approach, and suggests directions for further research.

6.1. Interpretation

Across all SSPs, the model consistently converges toward electrified configurations dominated by ASHP and GSHP-BTES systems, with only marginal supplemental use of NG. This leads to similar levels of emissions and similar operating system costs across all SSPs. Three primary mechanisms drive this convergence.

First, in warmer pathways (SSP3-7.0 and SSP5-8.5), the increasing frequency of warmer temperatures leads to a dominant need for cooling, reaching $\simeq 3\,\mathrm{GWh/yr}$ in SSP5-8.5 compared to $\leq 1\,\mathrm{GWh/yr}$ in SSP1-2.6. Cooling eventually becomes the leading source of operational costs, representing 68.8% of OPEX in SSP5-8.5 versus 24.8% in SSP1-2.6. Under the assumption of a carbon-neutral electricity grid by the century's end, cooling would be entirely decarbonized.

Second, the declining frequency of extreme cold days alters the cost-benefit equilibrium for peak heating capacity. As these events become rarer, the economic justification for investing in low-cost NG backup boilers diminishes. In carbon-constrained pathways (SSP1), high carbon prices further disincentivize NG, while in high-emission pathways (SSP5), the reduced need for backup heating makes it redundant. The required ASHP and GSHP capacity, already sized to meet peak cooling demand, can cover these infrequent heating peaks, even at a higher operational cost per event. However, even under mitigation scenarios, complete electrification is not achieved. Before the 2050s, this is due to relatively low carbon taxes and a still carbon-intensive grid. Later in the century, a marginal reliance on NG persists despite high carbon taxes, driven by the high cost of electricity and the low investment cost of an NG boiler. Notably, an electric-resistance boiler was available but remained unused throughout the study, indicating a clear cost preference for NG for this residual peaking role.

Third, BTES effectiveness increases across all SSPs as the seasonal temperature amplitude narrows. The rising frequency of warm days provides more excess summer heat for storage, improving winter utilization. This benefit is constrained only by the available drilling capacity and the finite energy suitable for inter-seasonal transfer. In practice, the carbon tax also incentivizes greater use of GSHP as a renewable, efficient heating technology.

In conclusion, this study demonstrates that future energy system configurations are profoundly shaped by climate change, and that today's socioeconomic choices—embodied in the SSPs—fundamentally determine their operational profile. Despite converging on similar system costs, carbon emissions, and technological designs (tailored to cope with extreme events), the resulting energy balance varies strongly across pathways. To achieve complete decarbonization, our findings suggest that policy measures such as banning new NG boiler installations or significantly increasing the cost of natural gas/decreasing the cost of electricity would be effective. Implementing nex taxes or bans would raise system operational costs by less than 20%, indicating a relatively modest economic trade-off for achieving full electrification and eliminating residual fossil fuel use.

6.2. Comparison with existing studies

The results confirm the pattern consistently reported in the literature: heating demand decreases and cooling demand increases under all climate scenarios. In Belgium, Elnagar et al. [3] projected a heating-demand reduction of 13–22% and a cooling-demand increase of 61–123% by the 2090s, using a detailed building-stock model that accounts for occupancy, internal gains, and ventilation. Our projections show the same qualitative trends but a wider quantitative range: heating demand declines between $-4\% \pm 23\%$ (SSP1-2.6) and $-57\% \pm 34\%$ (SSP5-8.5), while cooling demand rises by $+44\% \pm 26\%$ to $+291\% \pm 25\%$. This larger spread reflects our explicit treatment of structural uncertainty across multiple climate and policy pathways, rather than reliance on a single representative climate model.

Methodologically, the two studies differ in scope. Elnagar et al. [3] analyzed energy demand at the building and stock level, focusing on end-use dynamics. In contrast, our work links those climate-driven demand shifts to system-level investment and operation. By representing several long-term pathways of temperature and carbon-price evolution within a multi-stage planning framework, the model captures how district-scale technology choices and costs evolve across plausible futures. It therefore complements building-scale studies by translating projected demand changes into concrete system design and cost outcomes.

6.3. Limitations, and future work

Several methodological limitations qualify these conclusions. The model relies on linear programming and the use of typical days to represent temporal variability. This approach allows tractable optimization but under-represents short-term dynamics and extreme events.

From multi-stage to multi-horizons. In practice, the framework could be improved in both accuracy and speed through multi-horizon programming, which decouples the investment and operational subproblems. Such a formulation enables advanced decomposition algorithms, including adaptive oracles as introduced by Mazzi et al. [48] and Zhang et al. [49], and specialized bounding techniques such as those developed by Bayraksan et al. [50]. Improved convergence would also allow the inclusion of multiple operational scenarios per period, capturing the inter-model variability within each SSP, and facilitate the use of typical days instead of typical hours to represent more complex load profiles.

From one region to multi-region analysis. The case study reflects a temperate, heating-dominated climate. Results should therefore not be generalized without caution. In practice, our findings show that climate change does not impact significantly the cost stack for this specific case significantly because warmer temperatures reduce significantly heating requirements, improve the BTES balancing, and the overall performances of the ASHP and GSHP. However, this outcome does not hold in regions where cooling demand dominates or where loads are already balanced. In those contexts, higher ambient temperatures would likely increase electricity use and reduce system efficiency.

Enabling recourse in climate decision. Our use of four deterministic SSP branches, rather than a full multi-stage Markov chain, simplifies a core challenge of adaptive planning. While this choice limits the modeling of later-stage recourse between scenarios, it is justified by the physics of climate inertia—emissions pathways diverge into distinct, long-lived climatic states that cannot be seamlessly bridged mid-century. Moreover, integrated models currently lack dynamically branching scenarios for both climate and socioeconomic variables (e.g., carbon prices), which would be needed to represent such transitions. While multi-stage stochastic methods (e.g., using Markov chains to model evolving demand) exist, such as the district heating network adaptive planning by Kök et al. [9], these are not directly applicable to long-term climate uncertainty, as they do not address the specific physical irreversibility of warming trajectories. Our approach, therefore, focuses on the most decision-relevant uncertainty: ensuring first-stage infrastructure decisions are robust across the entire range of plausible, yet persistent, long-term futures, maintaining the relevance of our climate-motivated study.

Modelling of BTES for combined heating and cooling. Accurately modelling a storage system that serves both heating and cooling remains challenging. A physically detailed representation would require a multi-zone model that captures the BTES thermodynamics and adapts to varying supply temperatures, as explored in Wirtz et al. [51] and Hachez et al. [52]. However, the approach by Wirtz et al. [51] relies on a large number of integer variables to achieve physical fidelity; in addition to the computational burden, this approach is also unsuitable for storage sizing. This makes it unsuitable for our framework, which requires faster solutions and must also accommodate design optimisation. The alternative formulation by Hachez et al. [52] neglects inter-layer thermal losses, a key feature for any advanced BTES model. Consequently, we retain our simplified representation—which imposes limits on power and total energy transfer—and acknowledge this as an open research gap.

Thermal inertia as a source of flexibility. As renewable penetration grows and Belgium progresses toward Net-Zero, the assumption of constant electricity prices becomes increasingly inadequate. Although electricity tariffs in Belgium currently follow a monohorary structure (fixed within the contract period), this framework is being politically contested, and pending electricity-market reforms are expected to create more space for flexibility aggregators. Consequently, capturing the seasonal and intra-day variability of electricity prices—shaped by the evolving energy system—is gaining importance. A natural next step would be to integrate electricity-market dynamics into our thermal framework, leveraging campus thermal inertia and existing assets as flexibility resources. This could be complemented by adding new renewable capacity (e.g., waste- or biomass-fuelled CHP, PV panels) and exposing the system to a more volatile electricity market.

Sensitivity and Robustness Analysis. While this study provides a robust framework for sizing century-long infrastructure across divergent climate futures, a natural and valuable extension would be a comprehensive sensitivity and robustness analysis for non-climate related parameters, as done by Chaudhry et al. [53]. Future work could systematically vary key social, technical and economic parameters—such as unmet demand penalty, building insulation, ASHP/GSHP performance, BTES capacity and available power, and primary energy and carbon price trajectories—to quantify their individual and combined influence on the results. In particular, more flexible temperature requirements via a lower unmet demand penalty would provide interesting insights into the end-user flexibility's value.

Future work should extend the framework to a multi-horizon formulation that allows for adaptive investment decisions, integrate electricity system feedback and dynamic pricing, and test the methodology under contrasting climatic and load conditions. It should also include a purely simulation algorithm to include non-linear phenomenon, such as heat diffusion processes in BTES and practical considerations of a DHC, such as hydraulic simulations. Including demand-side flexibility, hybrid systems, and more detailed temporal representations would also further improve the realism and robustness of the results.

7. Conclusion

This paper introduced a multi-stage stochastic optimization framework to plan DHC systems under climate uncertainty. Using the SDDP algorithm, the model links uncertain climate evolution and CO_2 price trajectories to adaptive investment and operational strategies. This approach provides a century-scale perspective on how DHC systems can transition cost-effectively toward low-carbon configurations while remaining resilient across multiple socioeconomic pathways.

Applied to the Brussels campus case study, the analysis reveals two dominant trends: declining heat losses and rapidly growing heat gains. By 2100, heating needs fall by between $-4.0\% \pm 23\%$ under the sustainable pathway SSP1-2.6 and $-57\% \pm 34\%$ under the fossil-fueled development pathway SSP5-8.5. Over the same period, cooling demand increases by $+44\%\pm26\%$ and $+291\%\pm25\%$, respectively. These shifts fundamentally reshape the optimal technology mix. Across all scenarios, ASHP and GSHP-BTES become the backbone of the system, backed up by a NG. BTES enables seasonal balancing by storing excess summer heat for winter use, effectively providing efficient heating and cooling. Although NG boilers are installed to ensure reliability, their role is marginal and limited to short winter peaks.

The model shows that the mechanisms driving system transformation differ across scenarios, but converge toward similar electrified outcomes. In high-emission pathways (SSP3-7.0 and SSP5-8.5), rising temperatures improve the seasonal COP of heat pumps and reduce the frequency of extreme cold days, lowering the economic benefit of maintaining NG backup capacity. In mitigation pathways (SSP1-2.6 and SSP2-4.5), electrification is primarily driven by carbon pricing, which outweighs the short-term cost advantage of NG despite colder winter conditions relative to warmer scenarios. Across all pathways, OPEX stabilizes until the end of the century as improved heat pump efficiency and effective inter-seasonal storage for heating are counter-balanced by new cooling needs.

Overall, the results indicate that, in temperate and heating-dominated climates such as Belgium, electrified DHC systems with seasonal storage offer a robust, low-cost strategy under climate uncertainty. However, these conclusions should not be generalized to cooling-dominated regions, where rising temperatures could increase total electricity use and reduce overall system efficiency. Future work should extend this framework to multi-horizon adaptive planning, integrate feedback from electricity markets and dynamic pricing, and apply the model to contrasting climatic and demand contexts to assess its broader validity.

Credit author statement

Jonathan Hachez: Conceptualization, Investigation, Methodology, Writing - review & editing

Nicolas Ghilain: Data acquisition, Review

Ali Kök: Conceptualization, Methodology, Review

Diederik Coppitters: Conceptualization, Writing - review & editing

Acknowledgements

The authors gratefully acknowledge Pierre Gerard (VUB-ULB) for providing essential case study data and Nicolas Gaston for his valuable insights on borehole thermal modeling. This research was supported by the Research Foundation – Flanders (FWO) through a grant enabling Jonathan Hachez's scientific visit to TU Wien. Diederik Coppitters acknowledges support from the Fonds de la Recherche Scientifique - FNRS [CR 40016260]. The authors declare no competing financial interests or personal relationships that could have influenced the work presented in this paper.

Use of AI Tools

The authors employed several AI assistants—Claude (Anthropic), DeepSeek, ChatGPT (OpenAI), and Le Chat (Mistral)—to enhance the clarity and readability of both the manuscript and reviewer responses. These tools were also utilized for specific coding tasks, including figure formatting and data processing scripts. All core scientific content, including methodological design, analytical approaches, results interpretation, and conclusions, represents the original intellectual work of the authors. AI assistance was strictly limited to language refinement, presentation enhancement, and auxiliary programming tasks.

Code Availability

The CoolingClimate software package is openly available on GitHub at https://github.com/J0Hach3z/CoolingClimate/releases/tag/v0.0 under the MIT license. The v0.0 pre-release version used in this paper is archived there.

Figure A.11: Buildings and their period of construction [55]

Appendix A. Site description

Our case study takes place in Brussels, Belgium. As part of its urban plans, the city of Brussels agreed to let the former Ixelles Barracks become a new neighborhood. In the following sections, we detail the phases of the renovation project, the objectives of this renovation plan, and the impact on our study. [54]

Past and future of the site. The site transformation follows a multi-phase trajectory:

0. **Military Site (1906-2019):** The original “Ixelles Gendarmerie School," a closed-off military complex. During this period, the site was built gradually as depicted on Figure A.11
1. **Transitional Occupations (2019-2030):** First See-U, then UR Square, which temporarily activate the site with public, cultural, and innovative initiatives during renovation.
2. **Permanent Urban Development (2030+):** The definitive “Usquare.brussels" phase, guided by a Master Development Plan to create a permanent mixed-use neighborhood—the subject of this district heating case study.

Project goals. The renovation is guided by key sustainability and community objectives:

- **Social Mix & Openness:** Create an "open, mixed, university and international" district with public amenities and a new 2,000 m² park.

- **Innovation Hub:** Integrate academic research and public facilities like a FabLab.
- **Heritage & Sustainable Reuse:** Preserve historic architecture as a framework for low-carbon uses.
- **Sustainability & Livability:** Economize resources and ensure high quality of life.

Implications for the case study. The implications for the case study are fourfold.

- **Physics-driven model** Due to the ongoing renovation and fundamental change in effectuation, there is no access to relevant historical data. The long-term, multi-decade planning horizon under future climate conditions further precludes classical out-of-sample validation. As a result, we must rely on a physics-driven approach for demand estimation, and the credibility of our results depends on the internal consistency of the model, the use of physically and economically grounded assumptions, and the robustness of the solution under the prescribed uncertainty structure.
- **Retrofit** Due to the ongoing renovation, the envelope of the buildings will be additionally insulated. This retrofit leads us to assume a conductance of $U = 1.5\,\mathrm{W/m^2K}$ instead of the currently observed level.
- **District heating and cooling** The current centralized planning allows and includes the construction of a district heating and cooling network to control the heating and cooling supply. The layout will leverage two loops (one cold and one hot loop) in each trench (4 pipes) and supply the building on the main site. The insulation level for the pipes is such that the maximal losses are $0.37\,\mathrm{W/m\,K}$ [56]. The network will constitute approximately 700 m of trench [46], leading to losses approximating $1.036\,\mathrm{kW/K}$.
- **Borehole Thermal Energy storage** The planner wants to leverage the large empty spaces to drill boreholes in the area on three distinct locations. The borehole would be placed in a hexagonal disposition with a distance of 5 meters between each drill hole. The maximal number of boreholes is, for each field (7x2) + (14x2) + (10x9).

Appendix B. Timeserie aggregation

Typical days were constructed using TSAM aggregator. We used 16 design days, focusing on having representative temperature data, and averaging the related irradiance for every design day. the representative solar gains and temperature can be seen in Fig. B.13 and Fig. B.12.

We also put an emphasis on capturing extreme events and aggregating similar days according to the worst case for the cluster with the lowest and highest temperatures.

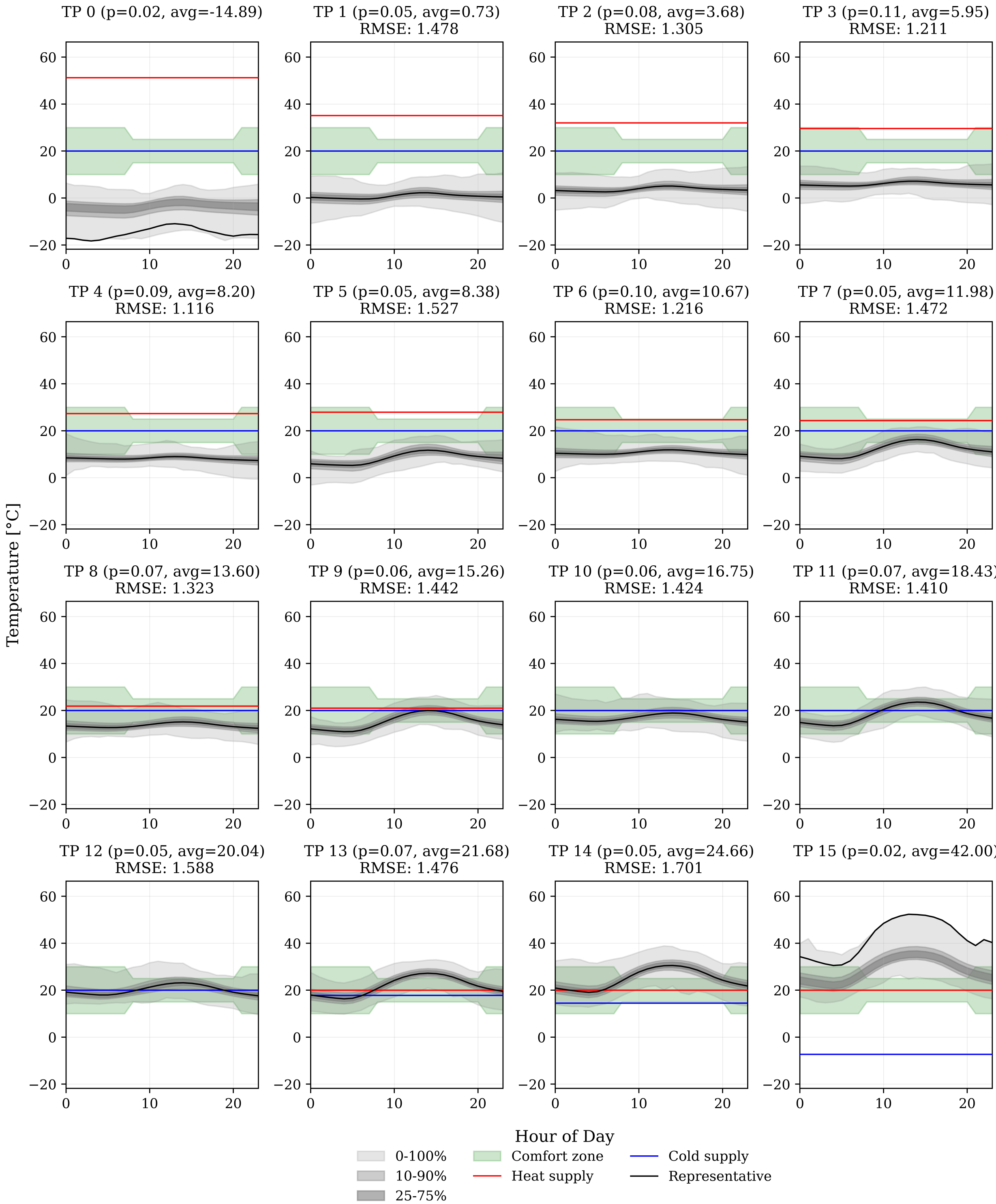

Figure B.12: Representation of temperature for every typical day. The first and last typical days are represented by their most extreme scenarios to enhance the robustness of the system and avoid smoothing out (solid black lines). The gray bands represent the distribution of the temperature for the days effectively represented by the black curve. The red and blue lines represent the supply temperature for heating and cooling, respectively, under these conditions.

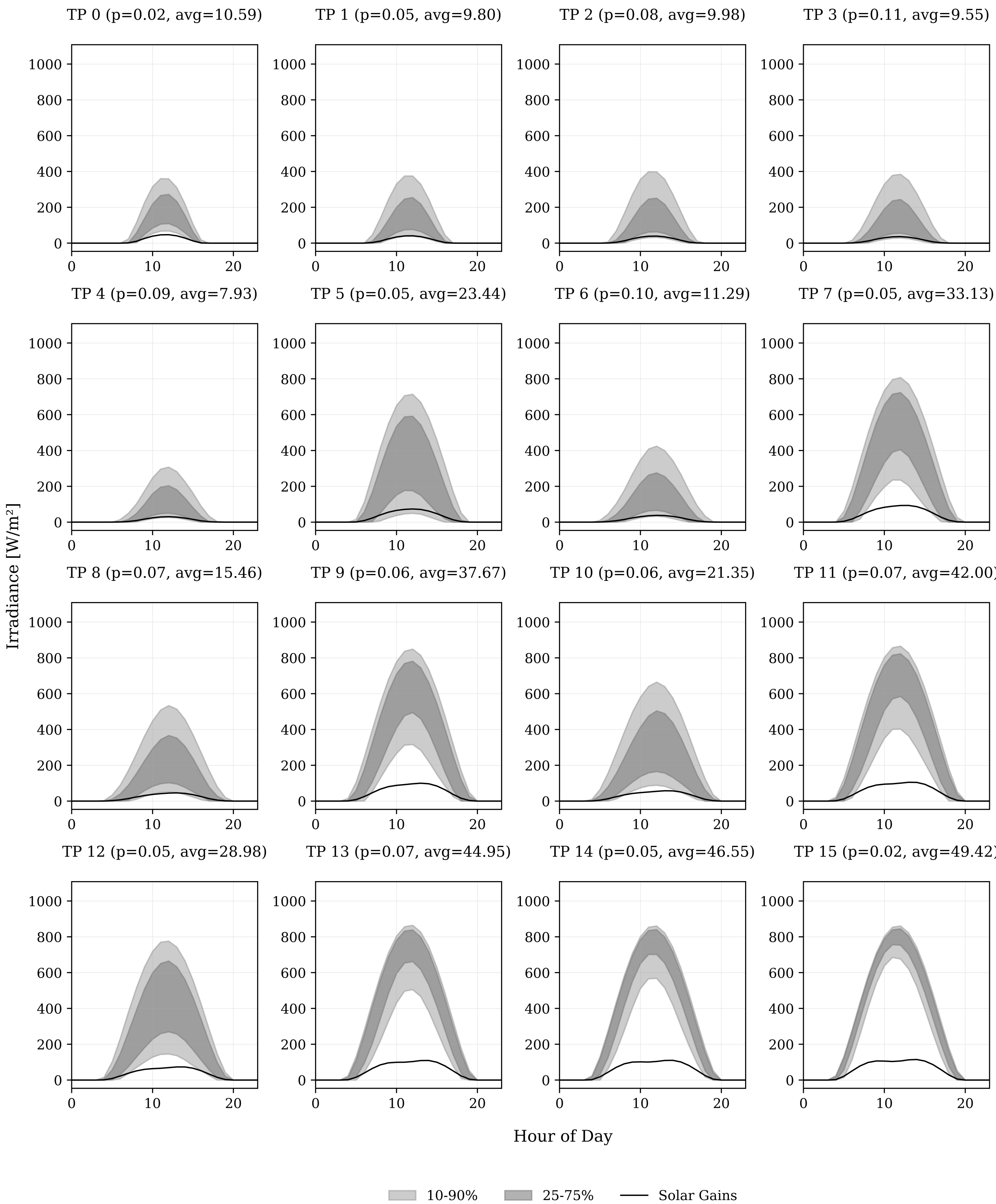

Figure B.13: Representation of the solar gains per square meter of glass, compared to the total irradiance on a horizontal surface per square meter. The gray bands represent the distribution of the irradiance values that are assumed to lead to the representative solar gains.

Appendix C. Operations modelling

Calculation of Supply Temperatures. The heating supply temperature T^{h}_{supply} and cooling supply temperature T^{c}_{supply} are computed based on time-dependent temperature thresholds and outdoor conditions. First, each hour is categorized as day (8–20 h) or night, with different minimum/maximum temperature limits (T_{min}, T_{max}) and building parameters. For each day, T^{h}_{supply} is determined as the maximum of $T_{min} + \max(0, T_{min} - T_{outdoor})$ across all hours, plus a 5°C margin. Similarly, T^{c}_{supply} is calculated as the minimum of $T_{max} - \max(0, T_{outdoor} - T_{max})$ for each day. These daily extremes ensure the supply temperatures meet the most demanding heating and cooling requirements while accounting for diurnal operational variations.

Assets conversion ability. For both heat pumps and natural boiler, we assume the regression performed in Appendix D.2 to hold. We compute the conversion factor from primary input to heating output as:

$$\mathrm{COP}^{\mathrm{h}}(T_{\mathrm{sink}}, T_{\mathrm{source}}) = a^{\mathrm{h}} \frac{T_{\mathrm{sink}} + 5\,\mathrm{K}}{T_{\mathrm{sink}} - T_{\mathrm{source}} + b^{\mathrm{h}}} \tag{C.1}$$

$$\mathrm{COP}^{\mathrm{c}}(T_{\mathrm{sink}}, T_{\mathrm{source}}) = a^{\mathrm{c}} \frac{T_{\mathrm{sink}} + 5\,\mathrm{K}}{T_{\mathrm{sink}} - T_{\mathrm{source}} + b^{\mathrm{c}}} - 1 \tag{C.2}$$

$$\eta_{\mathrm{NG\_boiler}}(T_{\mathrm{sink}}) = a^{\mathrm{NG\_boiler}} T_{\mathrm{sink}} - b^{\mathrm{NG\_boiler}} \tag{C.3}$$

$$\eta_{\mathrm{E\_boiler}} = 1.0 \tag{C.4}$$

For the geothermal system, we consider a constant temperature in the subsoil equal to 10 °C. For the conversion factor, we have:

$$\beta^{\mathrm{h}}_{\mathrm{ASHP},d,h} = \min(\mathrm{COP}^{\mathrm{h}}(T^{\mathrm{h}}_{\mathrm{supply},d}, T_{\mathrm{outdoor},d,h}), 8) \tag{C.5}$$

$$\beta^{\mathrm{c}}_{\mathrm{ASHP},d,h} = \min(\mathrm{COP}^{\mathrm{c}}(T_{\mathrm{outdoor},d,h}, T^{\mathrm{c}}_{\mathrm{supply},d}), 8) \tag{C.6}$$

$$\beta^{\mathrm{h}}_{\mathrm{GSHP},d,h} = \min(\mathrm{COP}^{\mathrm{h}}(T^{\mathrm{h}}_{\mathrm{supply},d}, 10\,^{\circ}\mathrm{C}), 15) \tag{C.7}$$

$$\beta^{\mathrm{c}}_{\mathrm{GSHP},d,h} = \min(\mathrm{COP}^{\mathrm{c}}(10\,^{\circ}\mathrm{C}, T^{\mathrm{c}}_{\mathrm{supply},d}), 15) \tag{C.8}$$

$$\beta^{\mathrm{c}}_{\mathrm{NG\_boiler},d,h} = \eta_{\mathrm{NG\_boiler}}(T^{\mathrm{h}}_{\mathrm{supply},d}) \tag{C.9}$$

$$\beta^{\mathrm{c}}_{\mathrm{E\_boiler},d,h} = \eta_{\mathrm{E\_boiler}} \tag{C.10}$$

Cost of primary resources. Based on the supplier tariff shown in Table C.2, we assumed the following cost for the primary resources:

$$c_{\mathrm{electricity}} = 268\,€/\mathrm{MWh} \tag{C.11}$$

$$c_{\mathrm{gas}} = 51\,€/\mathrm{MWh} \tag{C.12}$$

Table C.2: Current electricity and gas price decomposition tariffs from TotalEnergies, Jan 2026

Electricity (c€ /kWh)		**Gas (c€ /kWh)**	
Energy			
Energy price	11.76	Consumption	4.10
Green energy contribution – Brussels	2.23		
Transmission and distribution			
Distribution costs	9.39	Distribution costs – variable term	0.76
Transport	2.14	Transport	0.16
Taxes			
Energy contribution	0.19	Energy contribution	0.10
Federal excise duty (consumption-based)	1.14	Federal excise duty	0.07
Total	**26.85**	**Total**	**5.19**

Table C.3: Evolution of Electricity Generation Mix in Belgium (TWh) by Bureau fédéral du Plan [57]. The carbon intensity was computed assuming marginal emissions for Coal (820 $gCO2/kWh_e$), Natural Gas (490 $gCO2/kWh_e$), and Oil Products (650 $gCO2/kWh_e$). The rest of the mix is considered carbon neutral, and we assume carbon capture by 2050.

Generation Type	**2005**	**2030**	**2050**
Gross Electricity Production (TWh/yr)	**85.7**	**87.8**	**129.4**
Nuclear Energy	47.6	16.2	0.0
Renewable Energy Sources	3.0	49.2	85.9
Hydropower (excluding pumped storage)	2.5	2.9	0.8
Wind Energy	0.2	0.5	0.5
Solar Photovoltaic	0.3	34.7	66.9
Biomass + Waste	0.0	11.1	17.5
Geothermal	0.0	0.0	0.2
Coal	8.2	0.0	0.0
Natural Gas	25.1	22.5	43.5
Oil Products & Derived Gases	1.7	0.0	0.0
Carbon intensity (gCO2/kWh)	**235**	**154**	**0**[a]

[a]Assumed carbon capture

The operational costs depend on both the primary resource prices and a carbon tax reflecting the policy assumptions of each SSP. We apply different carbon intensities to the primary energy carriers: values computed in Table C.3 for electricity and a constant $200\,\mathrm{kg}_{\mathrm{CO}_2}/\mathrm{MWh}$ for natural gas. The resulting carbon cost term γ, which contributes to the total operational cost u, therefore varies by scenario ω and stage t, i.e., $\gamma = \gamma(\omega, t)$.

The evolution of the carbon tax over the century for each SSP (shown in Fig. C.14) is adapted from Riahi et al. [58]. This source provides explicit carbon price pathways for SSP1-2.6 and SSP2-4.5. For SSP3-7.0, where no direct estimate is available, the price is conservatively approximated as half of the value given for SSP3-6.0 in the same reference. For SSP5-8.5, a carbon price of zero is assumed. This is consistent with Riahi et al. [58]'s characterization of SSP5-8.5 as a baseline scenario reflecting historically implemented policies, where significant carbon taxation was absent. As this scenario assumes no new climate mitigation efforts, a zero carbon price is maintained in our projections through 2100.

Cost of unmet demand. The unmet-demand penalty reflects the strictness with which demand must be satisfied under all operational conditions. In this study, we set $u_{\text{unmet}} = 1\,\mathrm{M€/MWh}$. This choice effectively enforces demand satisfaction at all times and, as a result, leads to the systematic installation of peak NG boilers across most investment stages.

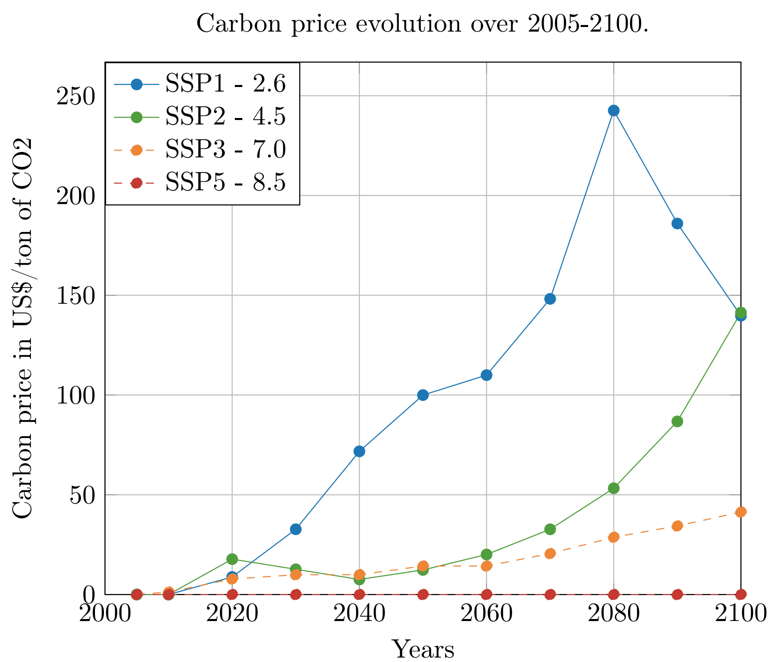

Figure C.14: Carbon price evolution over the century depending on the SSP, adapted from [58]. The carbon price for SSP3-7.0 was derived by taking half of the carbon price for SSP3-6.0 from Riahi et al. [58], and for SSP5-8.5, we take the carbon price would be zero.

Appendix D. Technology description

The technologies are detailed here, with their costs and operational characteristics. We assume most assets have a lifetime of 20 years (two stages), and the BTES has a lifetime of 50 years (five stages).

Appendix D.1. Technology Cost Projections

To model the evolution of energy technology investment costs over the planning horizon, we employ a hyperbolic decay function calibrated to the catalog data. The cost C_t of a given technology in year t is expressed as:

$$C_t = C_\infty + \frac{A}{t - t_0} \tag{D.1}$$

where C_∞ represents the asymptotic minimum cost (EUR/kW), A is a scaling parameter (EUR·year/kW), and t_0 is a year offset. Parameters are fitted via nonlinear least-squares optimization using from Prognos AG et al. [47] for each technology category (ASHP, NG boiler, PV, etc.). Future costs are then extrapolated through 2095.

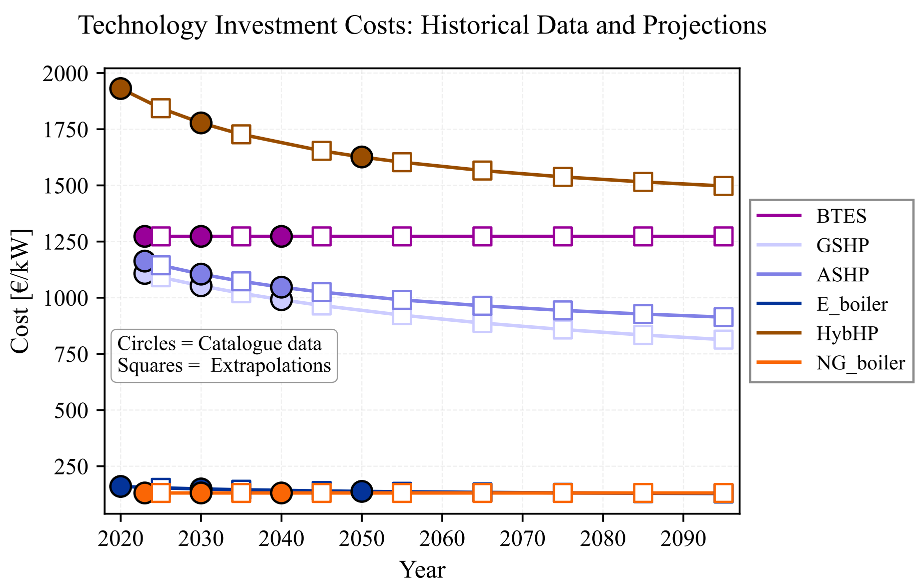

Figure D.15: Technology investment cost trajectories. Circles denote historical data points from Prognos AG et al. [47]; squares indicate decadal extrapolations (2025–2095). Solid lines show fitted hyperbolic decay curves, capturing technology learning rates and asymptotic cost floors.

The resulting projections (Fig. D.15) exhibit characteristic learning curves: steeper initial declines for emerging technologies (e.g., hybrid heat pump) versus flatter trajectories for mature assets (e.g., natural gas boilers). The hybrid heat pump is dominated by the ASHP + NG boiler combination, which leads us to rule it out.

To account for the long-term nature of infrastructure investments while operating within a finite planning horizon, our model applies a salvage value approach. This method accounts for investments made during the modeling period while cropping their remaining useful life and any end-of-life costs beyond the 2100 horizon (the remaining value of the assets at the end of the simulation period - called salvage value). By doing so, we ensure that cost comparisons between different technology pathways remain consistent and avoid distortions from post-horizon residual values or disposal costs.

Appendix D.2. Technology performance

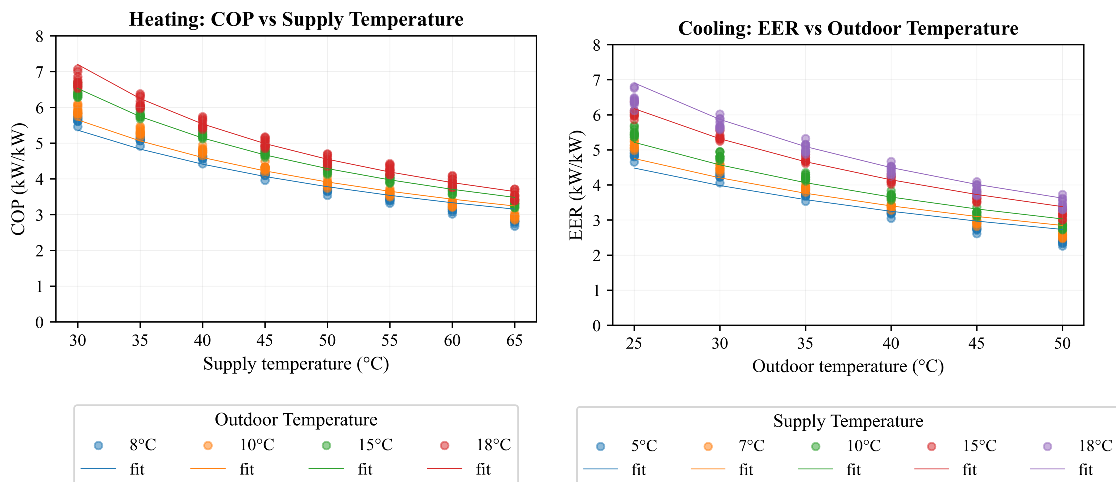

(a) Heating Coefficient of Performance (COP)

(b) Cooling Energy Efficiency Ratio (EER)

Figure D.16: Measured and fitted performance curves for a reversible heat pump. Scattered points represent manufacturer data, while solid lines show the fitted semi-empirical model. Fitting was performed using nonlinear least-squares optimization on manufacturer data across varying supply and outdoor temperatures.

Heat Pump Efficiency Analysis. The performance curves were fitted using a semi-empirical thermodynamic model derived from the Carnot efficiency principle. The heating COP and cooling EER are calculated from:

$$\mathrm{COP}_{\mathrm{heating}} = a_h \frac{T_h + 278.15}{T_h - T_c + b_h} \tag{D.2}$$

$$\mathrm{EER}_{\mathrm{cooling}} = a_c \frac{T_h + 278.15}{T_h - T_c + b_c} - 1 \tag{D.3}$$

where T_h and T_c are hot and cold side temperatures in °C. The fitted parameters are $a_h = 0.6815$, $b_h = 17.1753$ for heating and $a_c = 0.7656$, $b_c = 5.0000$ for cooling. These coefficients account for real-world irreversibilities and system losses relative to the ideal Carnot cycle. The model effectively captures the characteristic performance degradation with increasing temperature lift ($T_h - T_c$). The original data for the heat pump is taken from Carrier [59].

Boiler Efficiency Analysis. The efficiency variation of a boiler at part-load (30%) and full-load (100%) conditions was analyzed across supply temperatures from 40°C to 80°C. Figure D.17 presents the experimental data points alongside a linear regression for the full-load condition. The analysis reveals a strong negative correlation between supply temperature and efficiency, particularly at full load, where the relationship shows high predictability. This behavior indicates that higher supply temperatures reduce boiler efficiency, which should be considered in system optimization. The original data is from Viessmann [60].

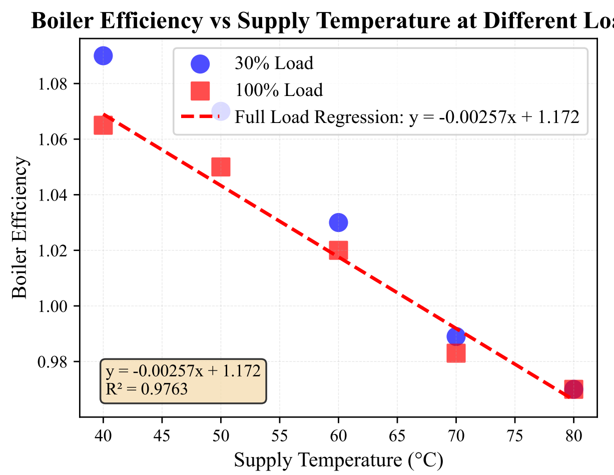

Figure D.17: Boiler efficiency versus supply temperature at 30% and 100% load conditions. Scatter points show experimental measurements, with the dashed line representing the linear regression for full-load operation. The regression equation and R^2 value are provided in the figure.

BTES. The borehole thermal energy storage system consists of 134 vertical boreholes, each 100 m deep, distributed over an area of 4350 m^2 and drilled through sand and quartz layers. The total subsurface volume affected by the borehole field is approximately 435 000 m^3. Each borehole provides an average thermal power of 6 kW, resulting in a total installed capacity of 804 kW. The surrounding subsurface material has a volumetric heat capacity of 2.3 $\mathrm{MJ\,m^{-3}\,K^{-1}}$, giving the system a total thermal storage capacity of approximately 1 $\mathrm{TJ\,K^{-1}}$, equivalent to 277 $\mathrm{MW\,h\,K^{-1}}$. This corresponds to a specific storage capacity of 344 $\mathrm{kW\,h\,kW^{-1}\,K^{-1}}$ per borehole. To maintain the annual ground temperature variation within an acceptable range of +/-2.5 °C (a 5 K interval), the annual heat injection into the storage is limited to 1.72 MW h per kW of installed capacity. In the model, this is implemented as a constraint where the total injected heat in kW h must not exceed $C = 1720$ times the installed thermal power in kW.

Nominal Load Efficiency Assumption. In energy systems, equipment efficiency typically changes when operating below its rated (nominal) capacity—a phenomenon known as part-load performance degradation for ASHP. On the contrary, this efficiency improves for NG, as one can observe in Fig. D.17, thanks to improved heat recuperation. However, for the long-term capacity planning model in this study, we assume all assets operate at their nominal (100%) power output and corresponding rated efficiency. This simplification is justified on two grounds. First, explicitly modeling the non-linear part-load curve would require integer variables, making the large-scale stochastic optimization problem computationally intractable. [61] Second, the assumption remains relevant at the system scale: modern equipment increasingly uses variable-speed drives that maintain high efficiency across a wide operating range, and systems in practice are composed of multiple modular units, allowing aggregate demand to be met by operating individual units near their optimal nominal point. Therefore, nominal efficiency provides a representative and computationally essential metric for infrastructure sizing under uncertainty.

Appendix E. Heat gains and losses

An overview of the heat gains and losses are visible on Fig. E.18 and Fig. E.19. We assume that those heat gains and losses impact the thermal inertia of the building $I = 2.4\,\mathrm{MW\,h\,K^{-1}}$

Wall losses. The wall losses have probably the most significant influence on the building indoor temperature. The combined envelope of the buildings amount to $40.000\,\mathrm{m}^2$ with an average thermal conductance of $u_{\mathrm{wall}} = 2.0\,\mathrm{W/m^2\,K}$ and a total conductance of $U_{\mathrm{wall}} = 80\,\mathrm{kW/K}$, exposed to the evolution of climate. The evolution of the yearly mean temperature is given at Fig. 2b. We provide, in addition, the inter-model distributions of the daily-averaged diurnal and nocturnal temperature per decade and SSP in Fig. 3.

Ventilation losses. The ventilation losses also dependent on temperature; the volume of air is estimated to $96\,000\,\mathrm{m}^3$, and the air renewal rate is set at 0.7 ACH during the day and 0.1 ACH during the night. The c_p of air is estimated to $1.2\,\mathrm{kJ/m^3\,K}$, leading to $U_{\mathrm{vent,day}} = 25.6\,\mathrm{kW/K}$ and $U_{\mathrm{vent,night}} = 3.2\,\mathrm{kW/K}$.

Solar gains. Solar gains were computed using hourly climate projections from multiple GCMs via the downward shortwave radiation. For each timestamp, the Sun's elevation angle was calculated using astronomical formulas adjusted for the site, day of year, and solar time. The effective solar gain penetrating the buildings' vertical wall was then derived by weighting the incident radiation considering the sun's angle relative to the surface, assuming the total glazing area $4 \times 10^3\,\mathrm{m}^2$ and that only half of it was exposed to the sun. $Q_{\mathrm{solar}} = I_{\mathrm{solar}} \cdot S_{\mathrm{glazen}}/2$.

Internal gains. The internal gains are assumed to be proportional to the living area, estimated to $35 \times 10^3\,\mathrm{m}^2$. The specific gains are quantified as $q_{\mathrm{int,day}} = 30\,\mathrm{W/m^2}$ during the day and $q_{\mathrm{int,night}} = 5\,\mathrm{W/m^2}$, leading to internal gains of $Q_{\mathrm{int,day}} = 1050\,\mathrm{kW}$ and $Q_{\mathrm{int,day}} = 175\,\mathrm{kW}$.

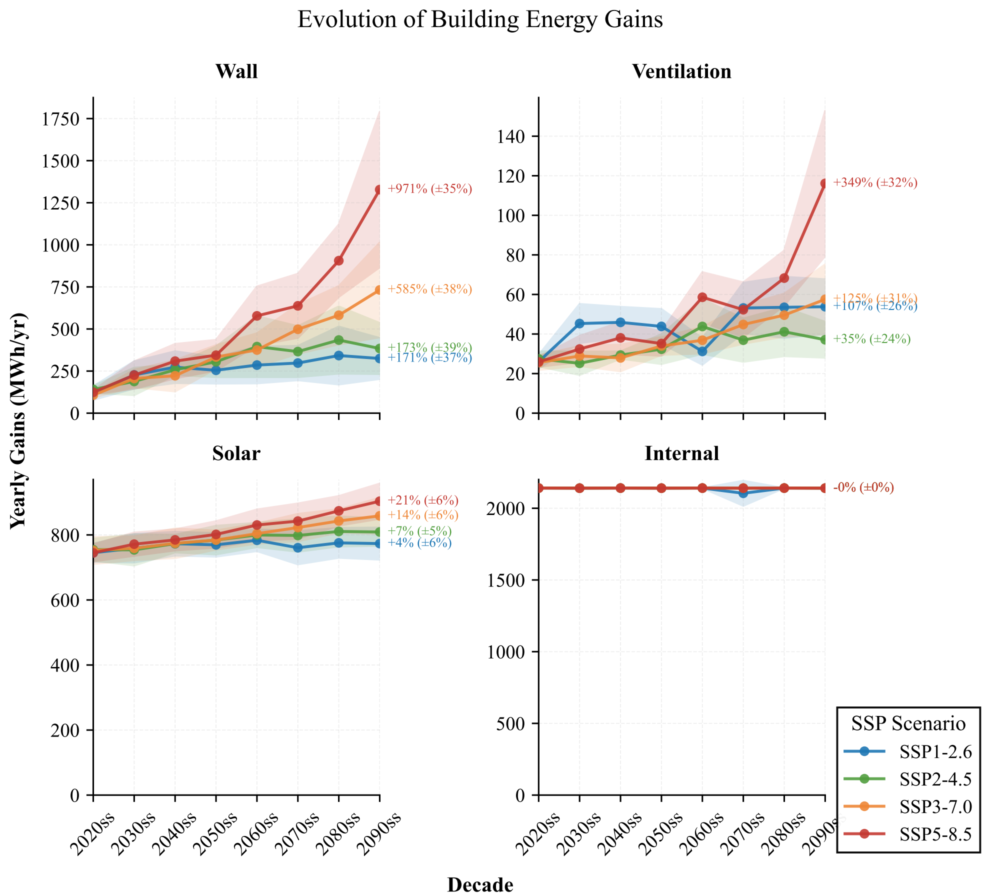

Figure E.18: Heat gains evolution per energy type

Network losses. The grid also has losses which needs to be accounted for when computing the losses. In practice, the planned insulation for the pipes is meant to bring the pipes losses to a maximum of $u_{\text{pipe}} = 0.37\,\text{W/m K}$ and we count 700 m of trench filled with 4 pipes each time (2 for cooling, 2 for heating), which means the heat and cold losses are brought to $U_{\text{pipe}} = 518\,\text{W/K}$ for each use (heating and cooling). Given the relative insignificance of this number in comparison to the other, we will neglect them.[11].

References

[1] Staffell, I., Pfenninger, S., Johnson, N.. A global model of hourly space heating and cooling demand at multiple spatial scales. Nature Energy 2023;8(12):1328–1344. doi:10.1038/s41560-023-01341-5.

[11]The network temperatures are relatively low, meaning the losses can clearly be neglected

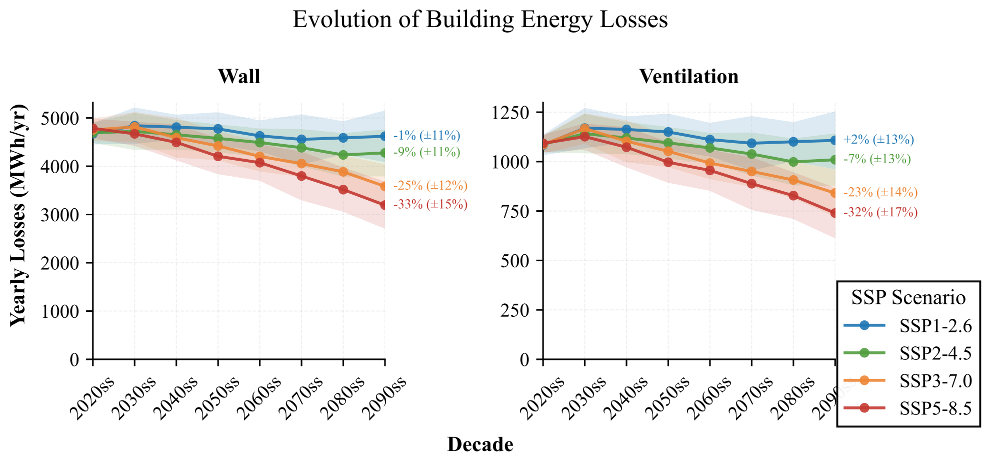

Figure E.19: Heat losses evolution per energy type

[2] Agency, I.E.. Buildings – Analysis. 2022. URL: https://www.iea.org/energy-system/buildings; accessed October 2025.

[3] Elnagar, E., Gendebien, S., Georges, E., Berardi, U., Doutreloup, S., Lemort, V.. Framework to assess climate change impact on heating and cooling energy demands in building stock: A case study of Belgium in 2050 and 2100. Energy and Buildings 2023;298:113547. doi:10.1016/j.enbuild.2023.113547.

[4] Mastrucci, A., van Ruijven, B., Byers, E., Poblete-Cazenave, M., Pachauri, S.. Global scenarios of residential heating and cooling energy demand and CO2 emissions. Climatic Change 2021;168(3-4):14. doi:10.1007/s10584-021-03229-3.

[5] Xiong, J., Guo, S., Wu, Y., Yan, D., Xiao, C., Lu, X.. Predicting the response of heating and cooling demands of residential buildings with various thermal performances in China to climate change. Energy 2023;269:126789. doi:10.1016/j.energy.2023.126789.

[6] Mutschler, R., Rüdisüli, M., Heer, P., Eggimann, S.. Benchmarking cooling and heating energy demands considering climate change, population growth and cooling device uptake. Applied Energy 2021;288:116636. doi:10.1016/j.apenergy.2021.116636.

[7] Cellura, M., Guarino, F., Longo, S., Tumminia, G.. Climate change and the building sector: Modelling and energy implications to an office building in southern Europe. Energy for Sustainable Development 2018;45:46–65. doi:10.1016/j.esd.2018.05.001.

[8] Baucke, R., Downward, A., Philpott, A.B.. Judge.jl: A julia package for optimizing capacity ex-

pansion. Optimization Online 2020;URL: https://optimization-online.org/?p=16779; published: 2020/11/02, Updated: 2021/04/19.

[9] Kök, A., Hachez, J., Kranzl, L.. A Multistage Stochastic Optimization Framework for Long-Term District Heating Capacity Expansion. In: 2025 21st International Conference on the European Energy Market (EEM). IEEE. ISBN 979-8-3315-1278-1; 2025, p. 1–8. doi:10.1109/EEM64765.2025.11050152.

[10] Dowson, O., Kapelevich, L.. <tt>SDDP.jl</tt> : A Julia Package for Stochastic Dual Dynamic Programming. INFORMS Journal on Computing 2021;33(1):27–33. doi:10.1287/ijoc.2020.0987.

[11] Siddique, M.B., Keles, D., Scheller, F., Nielsen, P.S.. Dispatch strategies for large-scale heat pump based district heating under high renewable share and risk-aversion: A multistage stochastic optimization approach. Energy Economics 2024;136:107764.

[12] Zwickl-Bernhard, S., Long, N., Jordan, S., Bauer, F., Simpson, J.G., Trainor-Guitton, W.. Optimizing district energy systems under uncertainty: Insights from a case study from Washington D.C., USA. Energy Conversion and Management 2025;341:119979. doi:10.1016/j.enconman.2025.119979.

[13] Shen, X., Luo, Z., Xiong, J., Liu, H., Lv, X., Tan, T., et al. Optimal Hybrid Energy Storage System Planning of Community Multi-Energy System Based on Two-Stage Stochastic Programming. IEEE Access 2021;9:61035–61047. doi:10.1109/ACCESS.2021.3074151.

[14] Chen, C., Sun, H., Shen, X., Guo, Y., Guo, Q., Xia, T.. Two-stage robust planning-operation co-optimization of energy hub considering precise energy storage economic model. Applied Energy 2019;252:113372. doi:10.1016/j.apenergy.2019.113372.

[15] Džiuvė, V., Lekavičius, V.. Planning the development of district heating in the face of uncertainty. Energy 2025;335:137894. doi:10.1016/j.energy.2025.137894.

[16] Grecu, N., Strömer, S., Schmidt, R.R., Maggauer, K., Marx, N., Mayr, B., et al. Decarbonizing a Polish district heating network using ambient and waste heat: a techno-economic analysis considering uncertainties in future energy prices and availability. Energy 2025;329:136641. doi:10.1016/j.energy.2025.136641.

[17] Petkov, I., Mavromatidis, G., Knoeri, C., Allan, J., Hoffmann, V.H.. MANGOret: An optimization framework for the long-term investment planning of building multi-energy system and envelope retrofits. Applied Energy 2022;314:118901. doi:10.1016/j.apenergy.2022.118901.

[18] Fiorentini, M., Heer, P., Baldini, L.. Design optimization of a district heating and cooling system with a borehole seasonal thermal energy storage. Energy 2023;262:125464.

[19] Deroubaix, A., Labuhn, I., Camredon, M., Gaubert, B., Monerie, P.A., Popp, M., et al. Large uncertainties in trends of energy demand for heating and cooling under climate change. Nature Communications 2021;12(1):5197. doi:10.1038/s41467-021-25504-8.

[20] Labriet, M., Joshi, S.R., Vielle, M., Holden, P.B., Edwards, N.R., Kanudia, A., et al. Worldwide impacts of climate change on energy for heating and cooling. Mitigation and Adaptation Strategies for Global Change 2015;20(7):1111–1136. doi:10.1007/s11027-013-9522-7.

[21] Larsen, M., Petrović, S., Radoszynski, A., McKenna, R., Balyk, O.. Climate change impacts on trends and extremes in future heating and cooling demands over Europe. Energy and Buildings 2020;226:110397. doi:10.1016/j.enbuild.2020.110397.

[22] Spinoni, J., Vogt, J.V., Barbosa, P., Dosio, A., McCormick, N., Bigano, A., et al. Changes of heating and cooling degree-days in Europe from 1981 to 2100. International Journal of Climatology 2018;38(S1). doi:10.1002/joc.5362.

[23] Olonscheck, M., Holsten, A., Kropp, J.P.. Heating and cooling energy demand and related emissions of the German residential building stock under climate change. Energy Policy 2011;39(9):4795–4806. doi:10.1016/j.enpol.2011.06.041.

[24] Wehrli, K., Sidler, F., Gubler, S., Settembrini, G., Koschenz, M., Domingo Irigoyen, S., et al. Building design in a changing climate – Future Swiss reference years for building simulations. Climate Services 2024;34:100448. doi:10.1016/j.cliser.2024.100448.

[25] Andrade, C., Mourato, S., Ramos, J.. Heating and Cooling Degree-Days Climate Change Projections for Portugal. Atmosphere 2021;12(6):715. doi:10.3390/atmos12060715.

[26] Walch, A., Li, X., Chambers, J., Mohajeri, N., Yilmaz, S., Patel, M., et al. Shallow geothermal energy potential for heating and cooling of buildings with regeneration under climate change scenarios. Energy 2022;244:123086. doi:10.1016/j.energy.2021.123086.

[27] Ziemele, J., Gendelis, S., Dace, E.. Impact of global warming and building renovation on the heat demand and district heating capacity: Case of the city of Riga. Energy 2023;276:127567.

[28] Ahmed, N.Y., Martínez, F.J.R., Hernández, J.M.R.. Climate-resilient zero energy buildings: Long-term modelling for energy efficiency and renewables impact. Results in Engineering 2025;27:106545. doi:10.1016/j.rineng.2025.106545.

[29] Tomrukcu, G., Ashrafian, T.. Climate-resilient building energy efficiency retrofit: Evaluating climate change impacts on residential buildings. Energy and Buildings 2024;316:114315. doi:10.1016/j.enbuild.2024.114315.

[30] Guarino, F., Tumminia, G., Longo, S., Cellura, M., Cusenza, M.A.. An integrated building energy simulation early—Design tool for future heating and cooling demand assessment. Energy Reports 2022;8:10881–10894. doi:10.1016/j.egyr.2022.08.224.

[31] Rodrigues, E., Fernandes, M.S.. Overheating risk in Mediterranean residential buildings: Comparison of current and future climate scenarios. Applied Energy 2020;259:114110. doi:10.1016/j.apenergy.2019.114110.

[32] Vidrih, B., Medved, S.. The effects of changes in the climate on the energy demands of buildings. International Journal of Energy Research 2008;32(11):1016–1029. doi:10.1002/er.1410.

[33] Thapa, S., Rijal, H.B., Pasut, W., Singh, R., Indraganti, M., Bansal, A.K., et al. Simulation of thermal comfort and energy demand in buildings of sub-Himalayan eastern India - Impact of climate change at mid (2050) and distant (2080) future. Journal of Building Engineering 2023;68:106068. doi:10.1016/j.jobe.2023.106068.

[34] Aram, K., Taherkhani, R., Šimelytė, A.. Multistage Optimization toward a Nearly Net Zero Energy Building Due to Climate Change. Energies 2022;15(3):983. doi:10.3390/en15030983.

[35] Hosseini, M., Javanroodi, K., Nik, V.M.. High-resolution impact assessment of climate change on building energy performance considering extreme weather events and microclimate – Investigating variations in indoor thermal comfort and degree-days. Sustainable Cities and Society 2022;78:103634. doi:10.1016/j.scs.2021.103634.

[36] Bazazzadeh, H., Pilechiha, P., Nadolny, A., Mahdavinejad, M., Hashemi safaei, S.s.. The Impact Assessment of Climate Change on Building Energy Consumption in Poland. Energies 2021;14(14):4084. doi:10.3390/en14144084.

[37] P. Tootkaboni, M., Ballarini, I., Corrado, V.. Analysing the future energy performance of residential buildings in the most populated Italian climatic zone: A study of climate change impacts. Energy Reports 2021;7:8548–8560. doi:10.1016/j.egyr.2021.04.012.

[38] Rey-Hernández, J.M., Yousif, C., Gatt, D., Velasco-Gómez, E., San José-Alonso, J., Rey-Martínez, F.J.. Modelling the long-term effect of climate change on a zero energy and carbon dioxide building through energy efficiency and renewables. Energy and Buildings 2018;174:85–96. doi:10.1016/j.enbuild.2018.06.006.

[39] Nematchoua, M.K., Roshan, G.R., Tchinda, R., Nasrabadi, T., Ricciardi, P.. Climate change and its role in forecasting energy demand in buildings: A case study of Douala City, Cameroon. Journal of Earth System Science 2015;124(1):269–281. doi:10.1007/s12040-014-0534-9.

[40] Summa, S., Tarabelli, L., Ulpiani, G., Di Perna, C.. Impact of Climate Change on the Energy and Comfort Performance of nZEB: A Case Study in Italy. Climate 2020;8(11):125. doi:10.3390/cli8110125.

[41] Birge, J.R., Louveaux, F.. Introduction to Stochastic Programming. 2nd ed.; New York: Springer; 2011. doi:10.1007/978-1-4614-0237-4.

[42] Philpott, A.B., Guan, Z.. On the convergence of stochastic dual dynamic programming and related methods. Operations Research Letters 2008;36(4):450–455. doi:10.1016/J.ORL.2008.01.013.

[43] Kotzur, L., Markewitz, P., Robinius, M., Stolten, D.. Time series aggregation for energy system design: Modeling seasonal storage. Applied Energy 2018;213:123–135. doi:10.1016/j.apenergy.2018.01.023.

[44] Kotzur, L., Markewitz, P., Robinius, M., Stolten, D.. Time series aggregation for energy system design: Modeling seasonal storage. Applied Energy 2018;213:123–135. doi:10.1016/j.apenergy.2018.01.023.

[45] Kannengießer, T., Hoffmann, M., Kotzur, L., Stenzel, P., Schuetz, F., Peters, K., et al. Reducing Computational Load for Mixed Integer Linear Programming: An Example for a District and an Island Energy System. Energies 2019;12(14):2825. doi:10.3390/en12142825.

[46] Anyoji Beltrando Architectes Urbanistes, , OLM paysagistes, , ON agence, , Studiebureau Jouret, , MK Engineering, . Aménagement des espaces publics de l'ancienne caserne d'ixelles / inrichting van de openbare ruimtes van de voormalige kazerne van elsene. Tech. Rep.; SAU-MSI.brussels; Bruxelles; 2022. Plan issu du dossier d'appel d'offres, lot 1 – Infrastructuur, réseau de chaleur avec bâtiment R (330_CH 100 R).

[47] Prognos AG, , ifeu – Institut für Energie- und Umweltforschung Heidelberg gGmbH, , Universität Stuttgart, Institut für Energiewirtschaft und Rationelle Energieanwendung (IER), . Impressum zum Technikkatalog Wärmeplanung. Tech. Rep.; Prognos AG; ifeu; IER, Universität Stuttgart; 2024. Auftraggeber: Bundesministerium für Wirtschaft und Klimaschutz (BMWK) und Bundesministerium für Wohnen, Stadtentwicklung und Bauwesen (BMWSB). Autorinnen und Autoren: Nora Langreder, Frederik Lettow, Malek Sahnoun, Sven Kreidelmeyer, Aurel Wünsch, Saskia Lengning, Sebastian Lübbers, Nils Thamling, Inka Ziegenhagen, Marco Wünsch, Dr. Sara Ortner, Angelika Paar, Lea Johannsen, Peter Mellwig, Benjamin Ott, Prof. Dr. Peter Radgen. Hinweise zu Hintergründen und Datenquellen sind im Begleitdokument zu finden.

[48] Mazzi, N., Grothey, A., McKinnon, K., Sugishita, N.. Benders decomposition with adaptive oracles for large scale optimization. Mathematical Programming Computation 2021;13(4):683–703. doi:10.1007/s12532-020-00197-0.

[49] Zhang, H., Mazzi, N., McKinnon, K., Nava, R.G., Tomasgard, A.. A stabilised Benders decomposition with adaptive oracles for large-scale stochastic programming with short-term and long-term uncertainty. Computers & Operations Research 2024;167:106665. doi:10.1016/j.cor.2024.106665.

[50] Bayraksan, G., Maggioni, F., Faccini, D., Yang, M.. Bounds for Multistage Mixed-Integer Distributionally Robust Optimization. SIAM Journal on Optimization 2024;34(1):682–717. doi:10.1137/22M147178X.

[51] Wirtz, M., Neumaier, L., Remmen, P., Müller, D.. Temperature control in 5th generation district heating and cooling networks: An MILP-based operation optimization. Applied Energy 2021;288. doi:10.1016/j.apenergy.2021.116608.

[52] Hachez, J., Latiers, A., Berger, B., Bram, S.. Multi-energy systems fast optimization: A new formulation in linear programming for temperatures and magnitudes of thermal power flows in heating systems. Energy and Buildings 2025;336:115618. doi:10.1016/j.enbuild.2025.115618.

[53] Chaudhry, A.M., Hachez, J., Chicherin, S., Ghorbaniasl, G., Bram, S.. Potential site evaluation of fifth-generation district heating and cooling networks under uncertain energy market conditions: A two-step robust design analysis approach. Energy 2024;311:133334. doi:10.1016/j.energy.2024.133334.

[54] Deneubourg, M., Bonhomme, G.. Casernes d'ixelles - usquare — perspective.brussels. https://perspective.brussels/fr/projets/poles-strategiques/casernes-dixelles-usquare; 2020. [Accessed 23-12-2025].

[55] MSA, , Idea Consult, , Origin, . étude de définition pour la reconversion de l'ancienne école de gendarmerie d'ixelles. Tech. Rep.; SPRB -Développement urbain Direction Etudes et Planification; Bruxelles; 2016. Etude réalisée à la demande de Bruxelles Développement Urbain-Service public régional de Bruxelles.

[56] ANYOJI BELTRANDO architectes urbanistes, , OLM paysagistes, , ON agence, , Studiebureau Jouret, , MK Engineering, . Usquare.brussels – cahier des charges techniques, lot 1 : Infrastructures. réseau de chaleur. Tech. Rep.; SAU-MSI.brussels; Bruxelles; 2022. Dossier de mise en concurrence – Lot 1 – Infrastructures. Cahier des charges du réseau de chaleur.

[57] Bureau fédéral du Plan, . Scénarios de choix énergétiques pour atteindre la neutralité climatique en 2050. 2024. URL: https://www.plan.be/fr/publications/scenarios-de-choix-energetiques-pour-atteindre-la; communication de presse, doc.id: PRESS_20240521.

[58] Riahi, K., van Vuuren, D.P., Kriegler, E., Edmonds, J., O'Neill, B.C., Fujimori, S., et al. The Shared Socioeconomic Pathways and their energy, land use, and greenhouse gas emissions implications: An overview. Global Environmental Change 2017;42:153–168. doi:10.1016/j.gloenvcha.2016.05.009.

[59] Carrier, . 61WG / 30WG Water-Sourced Liquid Chillers and Heat Pumps; n.d. Technical datasheet.

[60] Viessmann, . VIESMANN VITOCROSSAL 200 Gas Condensing Boiler, Type CM2. Viessmann Werke GmbH & Co KG; 2019. Gas condensing boiler for natural gas E, LL and LPG P; with modulating MatriX cylinder burner.

[61] Romberg, H., Höges, C., Graessner, R., Vering, C., Müller, D.. Towards optimal heat pump design: Integrating and investigating part-load behaviour. In: Proceedings of the 38th International Conference on Efficiency, Cost, Optimization, Simulation and Environmental Impact of Energy Systems (ECOS 2025). 2025,E.ON Energy Research Center; Chair of Energy Efficient Buildings and Indoor Climate.